ADHESIVE CONTACT OF A CONICAL FRUSTUM PUNCH WITH

A TRANSVERSELY ISOTROPIC OR AN ORTHOTROPIC

ELASTIC HALF SPACE

A Thesis

by

CHUNLIU MAO

Submitted to the Office of Graduate Studies of
Texas A&M University
in partial fulfillment of the requirements for the degree of

MASTER OF SCIENCE

December 2010

Major Subject: Mechanical Engineering

ADHESIVE CONTACT OF A CONICAL FRUSTUM PUNCH WITH

A TRANSVERSELY ISOTROPIC OR AN ORTHOTROPIC

ELASTIC HALF SPACE

A Thesis

by

CHUNLIU MAO

Submitted to the Office of Graduate Studies of
Texas A&M University
in partial fulfillment of the requirements for the degree of

MASTER OF SCIENCE

Approved by:

Chair of Committee,	Xin-Lin Gao
Committee Members,	Hong Liang
	Rashid Abu Al-Rub
Head of Department,	Dennis O'Neal

December 2010

Major Subject: Mechanical Engineering

ABSTRACT

Adhesive Contact of a Conical Frustum Punch with a Transversely Isotropic or an

Orthotropic Elastic Half Space. (December 2010)

Chunliu Mao, B.S., Harbin Engineering University, Heilongjiang, China

Chair of Advisory Committee: Dr. Xin-Lin Gao

The adhesive contact problems of a conical frustum punch indenting a transversely isotropic elastic half space and an orthotropic elastic half space are analytically studied in this thesis work. To solve the problem involving a transversely isotropic half space, the harmonic potential function method and the Hankel transform are employed, which lead to a general closed-form solution for the adhesive contact problem. For the case with an orthotropic half space, the problem of a point load applied on the half space is first solved by using the double Fourier transform method. The solution for the adhesive contact problem is then obtained through integrating the former solutions over the punch surface.

ACKNOWLEDGEMENTS

I want to thank my advisor, Dr. Xin-Lin Gao, for his patience and guidance. I learned how to do the research professionally. Without him, I would have had no chance to finish my thesis work.

I also would like to thank my committee members, Dr. Hong Liang and Dr. Abu Al-Rub, for their help and kindness.

I also want to thank my parents and my husband for their love and support.

TABLE OF CONTENTS

LIST OF FIGURES

LIST OF TABLES

CHAPTER I

INTRODUCTION

1.1.   Background

Solutions of contact problems have played an important role in many applications. In 1882, Hertz [1] developed a theory for spherical elastic bodies in contact under a pair of compressive forces, in which a half-ellipsoidal pressure distribution in the contact zone is assumed. However, Hertz's theory does not consider the adhesive interactions between the two contacting bodies inside and outside the contact zone. The other is that, the interaction outside the contact zone is not considered. Bradley [2] studied the adhesive contact between two contacting spheres by considering surface deformations. However, the surface energy and strength of the adhesion are not always directly related due to different geometries and other prescribed conditions.

Johnson et al. [3] developed an adhesive contact model, known as the JKR model, by considering the energy balance of the strain energy, potential energy and surface energy. The interacting force inside the contact area is shown to be larger than the one calculated using the Hertzian contact model.

Derjaguin et al. [4] proposed an adhesive contact model, called the DMT model, by introducing the molecular forces outside the contact region but assuming the Hertzian

---

This thesis follows the style of Journal of the Mechanics and Physics of Solids.

pressure distribution inside the contact zone. Both the JKR and DMT models have their limitations. The DMT model can be used for hard solids with low surface energy while, the JKR model fits soft materials with high surface energy better, e.g., Muller et al. [5]. This means that there should be a transition between the JKR and DMT models.

Maugis [6] developed a transition model, known as the MD model that bridges the JKR and DMT models.

A unified treatment of these and other existing contact models has recently been proposed by Zhou, Gao and He [7].

The three representative adhesive contact models, the JKR, DMT and MD models, have been used to study various indentation problems along with the non-adhesive contact theory of Hertz.

These models for isotropic materials are extended in the current thesis work to solve the contact problems of a conical frustum punch indenting an elastic half space that is transversely isotropic or orthotropic.

1.2. Motivation

The adhesionless contact problem of a flat-end conical punch indenting an isotropic elastic half space has been solved by Ejike [8]. However, the adhesive contact problem of a conical frustum punching a transversely isotropic or orthotropic elastic half space has not been solved. This motivated the current thesis work.

1.3. Organization

The detailed organization for the rest of the thesis is:

In Chapter II, the adhesive contact problem of a conical frustum punch with a

transversely isotropic half space has been analytically studied. The Hertz contact has been formulated by introducing both displacement and stress methods. In the displacement method, two harmonic potential functions are used, while in the stress method, one harmonic potential function is used. In order to solve the expressions of the normal displacement, radial displacement, normal stress and total force in terms of those potential functions, the Hankel transform method is used in both displacement and stress methods. Then, a solution of the Boussinesq contact problem of a rectangular punch involving a transversely isotropic elastic half space is obtained by considering an external crack near the punch edges. According to the superposition principle, the MD adhesive contact model of the prescribed problem has been approached and the expressions of the penetration depth, normal stress on the plane $z = 0$, the normal displacement on the plane $z = 0$ and the total force are obtained.

In Chapter III, the adhesive contact problem of a conical frustum punch with an orthotropic elastic half space has been solved. The problem of a point load applied on the half space is first solved by using the double Fourier transform method. Then, the adhesive contact solution of a conical frustum punch indenting a general orthotropic elastic half space is studied by assuming the pressure distribution of the JKR model.

CHAPTER II

ADHESIVE CONTACT OF A CONICAL

FRUSTUM PUNCH WITH A

TRANSVERSELY ISOTROPIC ELASTIC

HALF SPACE

2.1. Introduction

Elliott [9,10] studied the adhesionless contact problem of a transversely isotropic material indented by a conical, spherical or cylindrical punch by using a displacement formulation and the Hankel transform method. Hanson [11] further investigated the indentation of a transversely isotropic material by a conical punch by considering both the normal and tangential loadings. However, the adhesive interactions were not considered in [9-11].

Chen et al. [12] proposed a non-slipping JKR model for a transversely isotropic cylinder in contact with a dissimilar transversely isotropic elastic half space. However, the problem studied in [12] is only a plane strain problem.

Espinasse et al. [13] studied adhesive contact problems of transversely isotropic materials by extending the JKR and DMT models. But only a spherical punch is considered.

In this chapter, the adhesive contact problem of a conical frustum punch indenting a transversely isotropic elastic half space is studied. In Section 2.2, by using

displacement and stress methods, the closed-form solutions of the Hertz contact for the normal stress, the radial displacement, the normal displacement and total pressure are obtained. The Boussinesq contact problem of a rectangular punch is studied due to the singularity of an external crack near the punch edges. In Section 2.3, according to the superposition principle, the adhesive contact problem can consist of the Hertz contact and the Boussinesq contact problems, which are detailed in Section 2.4. Finally in Section 2.5, numerical results are shown by using selected transversely isotropic and isotropic materials.

Figure 2.1 schematically shows the adhesive contact of a rigid conical frustum punch with an elastic half space. The cylindrical coordinate system (r, θ, z) shown will be used. Under an external force P, the depth of penetration δ is reached by the punch whose profile is $f(r)$. The flat-end radius of the punch and contact radius are a_b and a, respectively. As indicated in Fig.2.1, α is the half-included angle of the conical frustum.
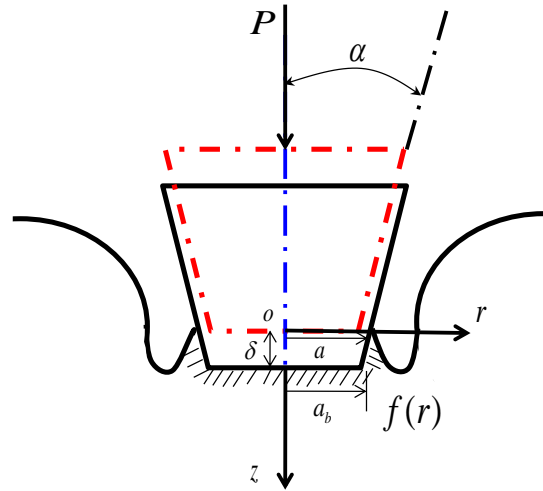
Fig. 2.1. Adhesive contact of a conical frustum punch with a transversely isotropic elastic half space

The boundary conditions for this adhesive contact problem are

$$\sigma_{zz} = 0,\, z = 0,\, r > a;$$
$$\sigma_{rz} = 0,\, z = 0,\, 0 < r < a; \qquad\qquad (2.1\text{a,b,c})$$
$$u_z = \delta - f(r),\, z = 0,\, 0 < r < a$$

The conical frustum punch profile is,

$$f(r) = \begin{cases} 0 & 0 \le r \le a_b \\ (r - a_b)\tan(\alpha) & a_b < r \le a \end{cases} \qquad\qquad (2.2\ \text{a,b})$$

2.2. The Hertz Contact for a Conical Frustum Punch

2.2.1 Displacement Method

The Hertz contact theory considers the contact problem without including any adhesive interaction. As a result, the configuration for the Hertz contact problem (see Fig.2.2) is different from that for the adhesive contact problem (see Fig.2.1).
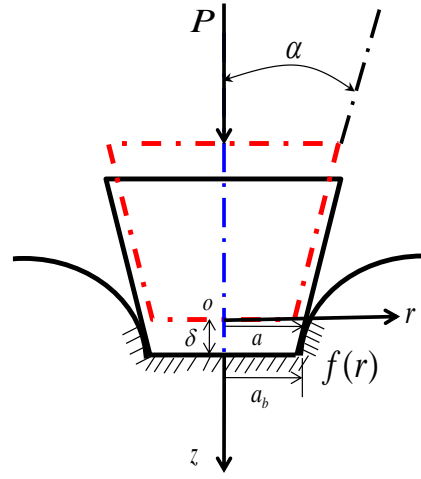
Fig. 2.2 Hertz contact of a conical frustum punch with a transversely isotropic elastic half space

For a transversely isotropic elastic half space (with $z > 0$), the stress-strain relations in the cylindrical coordinate system are given by Lai[14],

$$
\begin{aligned}
\sigma_{rr} &= c_{11}\varepsilon_{rr} + c_{12}\varepsilon_{\theta\theta} + c_{13}\varepsilon_{zz}, \\
\sigma_{\theta\theta} &= c_{12}\varepsilon_{rr} + c_{11}\varepsilon_{\theta\theta} + c_{13}\varepsilon_{zz}, \\
\sigma_{zz} &= c_{13}\varepsilon_{rr} + c_{13}\varepsilon_{\theta\theta} + c_{33}\varepsilon_{zz}, \\
\sigma_{\theta z} &= 2c_{44}\varepsilon_{\theta z}, \\
\sigma_{rz} &= 2c_{44}\varepsilon_{rz}, \\
\sigma_{r\theta} &= (c_{11} - c_{12})\varepsilon_{r\theta}.
\end{aligned}
\tag{2.3}
$$

The strain-displacement equations in the cylindrical coordinate system are,

$$\varepsilon_{rr} = \frac{\partial u_r}{\partial r}, \qquad \varepsilon_{\theta\theta} = \frac{1}{r}(u_r + \frac{\partial u_\theta}{\partial \theta}), \qquad \varepsilon_{zz} = \frac{\partial u_z}{\partial z},$$

$$\varepsilon_{\theta z} = \frac{1}{2}(\frac{\partial u_\theta}{\partial z} + \frac{1}{r}\frac{\partial u_z}{\partial \theta}),$$

$$\varepsilon_{rz} = \frac{1}{2}(\frac{\partial u_r}{\partial z} + \frac{\partial u_z}{\partial r}),$$

$$\varepsilon_{r\theta} = \frac{1}{2}(\frac{1}{r}\frac{\partial u_r}{\partial \theta} + \frac{\partial u_\theta}{\partial r} - \frac{u_\theta}{r}).$$

(2.4)

The current indentation problem is axi-symmetric with $u_\theta = 0$, $u_r = u_r(r,z)$, $u_z = u_z(r,z)$. Hence, Eq.(2.4) reduces to,

$$\varepsilon_{rr} = \frac{\partial u_r}{\partial r}, \qquad \varepsilon_{\theta\theta} = \frac{u_r}{r}, \qquad \varepsilon_{zz} = \frac{\partial u_z}{\partial z}, \quad \varepsilon_{rz} = \frac{1}{2}(\frac{\partial u_r}{\partial z} + \frac{\partial u_z}{\partial r}).$$

(2.5)

For the axi-symmetric problem with $\sigma_{r\theta} = 0, \sigma_{\theta z} = 0,$ and other $\sigma_{ij} = \sigma_{ij}(r,z)$, the equilibrium equations (in the absence of body forces) are given by,

$$\frac{\partial \sigma_{rr}}{\partial r} + \frac{1}{r}\frac{\partial \sigma_{r\theta}}{\partial \theta} + \frac{\partial \sigma_{rz}}{\partial z} + \frac{1}{r}(\sigma_{rr} - \sigma_{\theta\theta}) = 0,$$

$$\frac{\partial \sigma_{r\theta}}{\partial r} + \frac{1}{r}\frac{\partial \sigma_{\theta\theta}}{\partial \theta} + \frac{\partial \sigma_{\theta z}}{\partial z} + \frac{2}{r}\sigma_{r\theta} = 0,$$

$$\frac{\partial \sigma_{rz}}{\partial r} + \frac{1}{r}\frac{\partial \sigma_{\theta z}}{\partial \theta} + \frac{\partial \sigma_{zz}}{\partial z} + \frac{1}{r}\sigma_{rz} = 0.$$

(2.6)

By using Eqs. (2.3) and (2.5) into Eq.(2.6), the equilibrium equations can be written in terms of the displacements as

$$c_{11}(\frac{\partial^2 u_r}{\partial r^2} + \frac{1}{r}\frac{\partial u_r}{\partial r} - \frac{1}{r^2}u_r) + c_{13}\frac{\partial^2 u_z}{\partial r\partial z} + c_{44}(\frac{\partial^2 u_r}{\partial z^2} + \frac{\partial^2 u_z}{\partial r\partial z}) = 0,$$

$$c_{44}(\frac{\partial^2 u_r}{\partial r\partial z} + \frac{\partial^2 u_z}{\partial r^2}) + c_{13}\frac{\partial^2 u_r}{\partial r\partial z} + \frac{1}{r}(c_{13} + c_{44})\frac{\partial u_r}{\partial z} + c_{33}\frac{\partial^2 u_z}{\partial z^2} + \frac{c_{44}}{r}\frac{\partial u_z}{\partial r} = 0.$$

(2.7 a,b)

Following Elliott [9], the displacements u_r and u_z can be taken to have the form,

$$u_r = \frac{\partial \phi}{\partial r}, \qquad u_z = k \frac{\partial \phi}{\partial z} \tag{2.8}$$

where $\phi = \phi(r,z)$ and k is a constant.

inserting Eq. (2.8) into Eqs. (2.7 a,b) yields

$$c_{11}(\frac{\partial^2 \phi}{\partial r^2} + \frac{1}{r}\frac{\partial \phi}{\partial r}) + [k(c_{13}+c_{44})+c_{44}]\frac{\partial^2 \phi}{\partial z^2} = 0, \tag{2.9}$$

$$[c_{44}(1+k)+c_{13}](\frac{\partial^2 \phi}{\partial r^2} + \frac{1}{r}\frac{\partial \phi}{\partial r}) + c_{33}k\frac{\partial^2 \phi}{\partial z^2} = 0, \tag{2.10}$$

For eqns (2.9) and (2.10) to have a non-trivial solution, it is required that

$$\begin{vmatrix} c_{11} & k(c_{13}+c_{44})+c_{44} \\ c_{44}(1+k)+c_{13} & c_{33}k \end{vmatrix} = 0, \tag{2.11a}$$

which gives,

$$kc_{11}c_{33} - [k(c_{13}+c_{44})+c_{44}]\cdot[c_{44}(1+k)+c_{13}] = 0, \tag{2.11b}$$

Eq.(2.11b)can be rewritten as,

$$(c_{13}c_{44}+c_{44}^2)k^2 + (2c_{13}c_{44}+c_{13}^2+2c_{44}^2-c_{11}c_{33})k + c_{44}^2 + c_{13}c_{44} = 0, \tag{2.12}$$

which is a quadratic equation for k. Eq.(2.11b) can also be represented by

$$\frac{k(c_{13}+c_{44})+c_{44}}{c_{11}} = \frac{c_{33}k}{c_{44}(1+k)+c_{13}} = l, \tag{2.13a}$$

Eq.(2.13a) can be rewritten as

$$c_{11}c_{44}l^2 + [c_{13}(2c_{44}+c_{13})-c_{11}c_{33}]l + c_{33}c_{44} = 0, \tag{2.13b}$$

which is a quadratic equation for l.

Three possibilities can be considered for the roots of either Eq.(2.12) or equation (2.13): two distinct real roots; two identical real roots and two distinct complex roots. For the case of two distinct roots, the displacement method is used to solve the problem, while for the case of two identical roots, the stress method is chosen to solve the problem.

From Eqs.(2.10) or (2.11), it then follows that for each root l_i of Eq.(2.13b), the solution $\phi(r, z)$ satisfies

$$(\nabla_1^2 + l_i \frac{\partial^2}{\partial z^2})\phi_i = 0 \qquad (i = 1, 2), \tag{2.14}$$

where

$$\nabla_1^2 = \frac{\partial^2}{\partial r^2} + \frac{1}{r}\frac{\partial}{\partial r} \tag{2.15}$$

In terms of $\phi_i(r, z)$, the displacements given in Eq.(2.8) can now be expressed

$$u_r = \frac{\partial(\varphi_1 + \varphi_2)}{\partial r}, \qquad u_z = k_1 \frac{\partial \varphi_1}{\partial z} + k_2 \frac{\partial \varphi_2}{\partial z}, \tag{2.16a,b}$$

where k_1 and k_2 are the two roots of Eq.(2.12)

Using Eqs.(2.16a,b) and (2.5) in Eq.(2.3) then yields

$$\sigma_{rr} = c_{11} \frac{\partial^2(\varphi_1 + \varphi_2)}{\partial r^2} + \frac{c_{12}}{r} \frac{\partial(\varphi_1 + \varphi_2)}{\partial r} + c_{13}(k_1 \frac{\partial^2 \varphi_1}{\partial z^2} + k_2 \frac{\partial^2 \varphi_2}{\partial z^2}),$$

$$\sigma_{\theta\theta} = c_{12} \frac{\partial^2(\varphi_1 + \varphi_2)}{\partial r^2} + \frac{c_{11}}{r} \frac{\partial(\varphi_1 + \varphi_2)}{\partial r} + c_{13}(k_1 \frac{\partial^2 \varphi_1}{\partial z^2} + k_2 \frac{\partial^2 \varphi_2}{\partial z^2}),$$

$$\sigma_{zz} = c_{13} \frac{\partial^2(\varphi_1 + \varphi_2)}{\partial r^2} + \frac{c_{13}}{r} \frac{\partial(\varphi_1 + \varphi_2)}{\partial r} + c_{33}(k_1 \frac{\partial^2 \varphi_1}{\partial z^2} + k_2 \frac{\partial^2 \varphi_2}{\partial z^2}),$$

<div align="right">(2.16c-f)</div>

$$\sigma_{rz} = c_{44}[\frac{\partial^2(\varphi_1 + \varphi_2)}{\partial r \partial z} + k_1 \frac{\partial^2 \varphi_1}{\partial r \partial z} + k_2 \frac{\partial^2 \varphi_2}{\partial r \partial z}].$$

Define the potential functions ϕ_i by using Hankel transform below,

$$\phi_i = \int_0^\infty \xi G_i(\xi z_i) J_0(\xi r) d\xi, \quad i = 1, 2 \qquad (2.17a)$$

where, $J_0(\xi r)$ is the zeroth-order Bessel function of the first kind, $G_i(\xi z_i)$ are two functions yet unknown and

$$z_i = \frac{z}{\sqrt{l_i}} \qquad (2.17b)$$

using Eq. (2.17) in Eq.(2.14) gives,

$$\int_0^\infty \xi^3 [G_i''(\xi z_i) - G_i(\xi z_i)] J_0(\xi r) d\xi = 0, \qquad (2.18a)$$

which is satisfied when

$$G_i''(\xi z_i) - G_i(\xi z_i) = 0, \qquad (2.18b)$$

The general solution of Eq.(2.18b) is

$$G_i = A_i e^{-\xi z_i} + B_i e^{\xi z_i} \quad (i = 1, 2), \qquad (2.19a)$$

For the displacement and stress components to vanish at infinity, it requires that $G_i \to 0$ as $z \to \infty$. As a result, Eq.(2.19a) reduces to

$$G_i(\xi z_i) = A_i e^{-\xi z_i} \qquad (2.19b)$$

By using Eq. (2.17) in Eqs.(2.16c-f), gives the displacement and stress

components as

$$u_r = -\int_0^\infty \xi^2 (G_1 + G_2) J_1(\xi r) d\xi \qquad\qquad (2.20\text{a-f})$$

$$u_z = \int_0^\infty \xi (k_1 \frac{\partial G_1}{\partial z} + k_2 \frac{\partial G_2}{\partial z}) J_0(\xi r) d\xi$$

$$\sigma_{rr} = \int_0^\infty \{[c_{13}\xi(k_1 \frac{\partial^2 G_1}{\partial z^2} + k_2 \frac{\partial^2 G_2}{\partial z^2}) - c_{11}\xi^3(G_1 + G_2)] J_0(\xi r)$$
$$+ \frac{\xi^2}{r}(c_{11} - c_{12})(G_1 + G_2) J_1(\xi r)\} d\xi$$

$$\sigma_{zz} = \int_0^\infty \xi[(c_{33}k_1 - c_{13}l_1) \frac{\partial^2 G_1}{\partial z^2} + (c_{33}k_2 - c_{13}l_2) \frac{\partial^2 G_2}{\partial z^2}] J_0(\xi r) d\xi$$

$$\sigma_{\theta\theta} = \int_0^\infty \{[c_{13}\xi(k_1 \frac{\partial^2 G_1}{\partial z^2} + k_2 \frac{\partial^2 G_2}{\partial z^2}) - c_{12}\xi^3(G_1 + G_2)] J_0(\xi r)$$
$$+ \frac{\xi^2}{r}(c_{12} - c_{11})(G_1 + G_2) J_1(\xi r)\} d\xi$$

$$\sigma_{rz} = -\int_0^\infty \xi^2 c_{44}[(1+k_1) \frac{\partial G_1}{\partial z} + (1+k_2) \frac{\partial G_2}{\partial z}] J_1(\xi r) d\xi$$

From Eqs. (2.1b) and (2.19b),

$$\int_0^\infty \xi^3 c_{44}[(1+k_1) \frac{1}{\sqrt{l_i}} A_1 + (1+k_2) \frac{1}{\sqrt{l_2}} A_2] J_1(\xi r) d\xi = 0, \quad 0 < r < a \qquad (2.21)$$

Eq. (2.21) will be satisfied when

$$(1+k_1) \frac{1}{\sqrt{l_1}} A_1 + (1+k_2) \frac{1}{\sqrt{l_2}} A_2 = 0, \qquad\qquad (2.22)$$

which gives

$$A_1 = -\frac{1+k_2}{1+k_1}\sqrt{\frac{l_1}{l_2}}A_2 \tag{2.23}$$

using Eqs.(2.20e) and (2.19b) in Eq.(2.1 a)yields

$$\int_0^\infty \xi^3[(c_{33}k_1 - c_{13}v_1)(-\frac{1+k_2}{1+k_1})\frac{1}{\sqrt{l_1l_2}} + (c_{33}k_2 - c_{13}v_2)\frac{1}{l_2}]A_2(\xi)J_0(\xi r)d\xi = 0, r > a \tag{2.24}$$

Let,

$$D = (c_{33}k_1 - c_{13}l_1)(-\frac{1+k_2}{1+k_1})\frac{1}{\sqrt{l_1l_2}} + (c_{33}k_2 - c_{13}l_2)\frac{1}{l_2} \tag{2.25}$$

Eq. (2.24) then becomes

$$\int_0^\infty \xi^3 DA_2(\xi)J_0(\xi r)d\xi = 0, r > a \tag{2.26}$$

Similarly, from Eqs.(2.20b), (2.19b) and (2.23), the displacement in the z-direction on the plane $z = 0$ is obtained as

$$u_z(r,0) = -\int_0^\infty \xi^2(\frac{k_2-k_1}{1+k_1})\frac{1}{\sqrt{l_2}}A_2(\xi)J_0(\xi r)d\xi \tag{2.27}$$

Let

$$\xi a = p, \qquad r = a\tau,$$
$$-\frac{u_z(r,0)(1+k_1)D}{(k_2-k_1)a} = g\ (\tau), \tag{2.28a-d}$$
$$\frac{Dp^2A_2(\xi)}{\sqrt{l_2}a^4} = F\ (p),$$

Thus, Eqs.(2.26) and (2.27) can be written in term of the parameters defined in

Eq.(2.28)

$$\int_0^\infty F\ (p)J_0(p\tau)dp = g\ (\tau), \qquad 0 < \tau < 1$$

$$\int_0^\infty pF\ (p)J_0(p\tau)dp = 0, \qquad \tau > 1$$

(2.29a,b)

The dual equations given in Eqs.(2.29 a,b) have the following solution by Titchmarsh (1937)[15].

$$F\ (p) = \frac{2}{\pi}\cos(p)\int_0^1 y(1-y^2)^{-1/2}g(y)dy$$

$$+\frac{2}{\pi}\int_0^1 y(1-y^2)^{-1/2}dy\int_0^1 g(yu)pu\sin(pu)du$$

(2.30)

When $a_b \leq r < a$, $\dfrac{a_b}{a} \leq \tau < 1$, then the boundary condition in (2.1c) reads

$$u_z(r,0) = \delta\ - f(r) = \delta\ -(r-a_b)\tan(\alpha)$$

(2.31)

inserting Eq.(2.31) into Eq.(2.28c)

$$g\ (\tau) = -\frac{[\delta\ -(a\tau-a_b)\tan(\alpha)](1+k_1)D}{(k_2-k_1)a}$$

(2.32)

using Eq.(2.32) in Eq.(2.30) then yields

$$F\ (p) = \frac{2D(1+k_1)}{a\pi(k_2-k_1)}[\frac{\pi a}{2p}\tan(\alpha)\sin(p) - \frac{\delta\ \sin(p)}{p}$$

$$-\frac{a_b\tan(\alpha)\sin(p)}{p} - \frac{\pi a\tan(\alpha)}{2p^2} + \frac{\pi a\cos(p)\tan(\alpha)}{2p^2}]$$

(2.33)

substituting Eq.(2.33) into (2.28d) gives the expression of A_2 as

$$A_2 = \frac{a^4 \sqrt{l_2}}{Dp^2} F(p)$$

$$= \frac{2a^3 \sqrt{l_2}(1+k_1)}{\pi(k_2-k_1)p^2}[\frac{\pi a}{2p}\tan(\alpha)\sin(p) - \frac{\delta \sin(p)}{p}$$

$$- \frac{a_b \tan(\alpha)\sin(p)}{p} - \frac{\pi a \tan(\alpha)}{2p^2} + \frac{\pi a \cos(p)\tan(\alpha)}{2p^2}]$$

(2.34)

The use of Eqs. (2.34), (2.23), (2.19b) in Eq.(2.20a-f) will lead to the complete determination of the displacement and stress components. Inserting Eq.(2.33) into Eq.(2.29b) results in

$$\sigma_{zz}(a\tau,0) = \int_0^\infty pF\ (p)J_0(p\tau)dp$$

$$= \frac{2D(1+k_1)}{a\pi(k_2-k_1)}\int_0^\infty [\sin(p)(\frac{\pi a \tan(\alpha)}{2} - \delta\ - a_b \tan(\alpha))J_0(p\tau)dp$$

$$+ \int_0^\infty [\frac{\pi a \tan(\alpha)}{2}(\frac{\cos(p)-1}{p})]J_0(p\tau)dp = 0$$

(2.35a)

which indicates that each integral has to be finite at any $\tau \in [1,\infty)$ or $r \in [a,\infty)$. For the first integral to be finite at $\tau = 1$, it is necessary that (see Appendix A, Eq.(A2))

$$\frac{\pi a \tan(\alpha)}{2} - \delta\ - a_b \tan(\alpha) = 0,$$

(2.35b)

which gives the depth of the punch penetration as

$$\delta\ = \frac{\pi a \tan(\alpha)}{2} - a_b \tan(\alpha)$$

(2.35c)

using Eq.(2.35c) in Eq.(2.33) yields

$$F(p) = \frac{2D(1+k_1)}{(k_2-k_1)} \cdot \frac{\tan(\alpha)}{2} \cdot \frac{\cos p - 1}{p^2} \tag{2.36}$$

From Eqs.(2.20a,b,d), the normal stress, radial and normal displacements and the total force on the plane $z = 0$ can be obtained as

$$\sigma_{zz}(r,0) = -\frac{1+k_1}{k_2-k_1} D\tan(\alpha)\cosh^{-1}(a/r), \qquad a_b \le r < a \tag{2.37 a-d}$$

$$u_r(r,0) = \int_0^\infty F(p)J_1(p\tau)dp \cdot (\frac{1+k_2}{1+k_1}\sqrt{\frac{l_1}{l_2}} - 1)\frac{a}{D}$$

$$= \begin{cases} \dfrac{r\tan(\alpha)}{2}[\log(\dfrac{r}{a+\sqrt{a^2-r^2}}) - \dfrac{a^2-a\sqrt{a^2-r^2}}{r^2}] \cdot (\dfrac{1+k_2}{k_2-k_1}\sqrt{\dfrac{l_1}{l_2}} - \dfrac{1+k_1}{k_2-k_1}), & a_b \le r < a \\[4mm] -\dfrac{a^2}{2r}\tan(\alpha)(\dfrac{1+k_2}{k_2-k_1}\sqrt{\dfrac{l_1}{l_2}} - \dfrac{1+k_1}{k_2-k_1}), & r \ge a \end{cases}$$

$$u_z(r,0) = \begin{cases} \dfrac{\pi a\tan(\alpha)}{2} - r\tan(\alpha), & a_b \le r < a \\[4mm] a\tan(\alpha)[\sin^{-1}(\dfrac{a}{r}) + \sqrt{\dfrac{r^2}{a^2}-1} - \dfrac{r}{a}], & r \ge a \end{cases}$$

$$P_1 = -2\pi\int_{a_b}^a r\sigma_{zz}(r,0)dr$$

$$= -\frac{\pi D\tan(\alpha)(1+k_1)}{k_2-k_1}[a\sqrt{a^2-a_b^2} - a_b^2\cosh^{-1}(\frac{a}{a_b})], \qquad a_b \le r < a$$

In reaching Eqs.(2.37 a-d), use has been made of Eqs.A(1)-A(5) given in Appendix A.

For $0 \leq r < a_b$, or $0 \leq \tau < \dfrac{a_b}{a}$,

$$u_z(r,0) = \delta \qquad\qquad (2.38)$$

which is given in Eqs. (2.1c) and (2.2 a).

By following a procedure similar to that used for the region $a_b \leq r < a$, the solution for this case can be readily obtained to be

$$g(\tau) = -\frac{\delta (1+k_1)D}{(k_2 - k_1)a}, \qquad 0 \leq \tau < \frac{a_b}{a}$$

$$F(p) = -\frac{2D(1+k_1)}{a\pi(k_2 - k_1)} \cdot \frac{\sin(p)}{p}\delta, \qquad 0 \leq \tau < \frac{a_b}{a} \qquad (2.39 \text{ a,b})$$

Thus,

$$\sigma_{zz}(r,0) = -\frac{2D(1+k_1)}{\pi(k_2 - k_1)}\tan(\alpha)(\frac{\pi a}{2} - a_b)\frac{1}{\sqrt{a^2 - r^2}}, \qquad 0 \leq r < a_b \qquad (2.40\text{a-d})$$

$$u_r(r,0) = \int_0^\infty F(p)J_1(p\tau)dp \cdot (\frac{1+k_2}{1+k_1}\sqrt{\frac{l_1}{l_2}} - 1)\frac{a}{D}$$

$$= -\frac{2r\tan(\alpha)}{\pi}(\frac{\pi a}{2} - a_b) \cdot \frac{1}{a + \sqrt{a^2 - r^2}}(\frac{1+k_2}{1+k_1}\sqrt{\frac{l_1}{l_2}} - 1)(\frac{1+k_1}{k_2 - k_1}), \qquad 0 \leq r < a_b$$

$$u_z(r,0) = (\frac{\pi a}{2} - a_b)\tan(\alpha), \qquad 0 \leq r < a_b$$

$$P_2 = -2\pi \int_0^{a_b} r\sigma_{zz}(r,0)dr$$

$$= \frac{4D(1+k_1)}{k_2 - k_1}\tan(\alpha)(\frac{\pi a}{2} - a_b)(a - \sqrt{a^2 - a_b^2}), \qquad 0 \leq r < a_b$$

By combining the solutions derived above for the two regions, the normal stress,

radial and normal displacements and total force can be summarized as

$$\delta = (\frac{\pi a}{2} - a_b)\tan(\alpha),$$

<div align="right">(2.41a-e)</div>

$$\sigma_{zz}(r,0) = \begin{cases} -\dfrac{2D(1+k_1)}{\pi(k_2-k_1)}\tan(\alpha)(\dfrac{\pi a}{2}-a_b)\cdot\dfrac{1}{\sqrt{a^2-r^2}}, & 0 \le r < a_b \\[3mm] -\dfrac{(1+k_1)}{k_2-k_1}D\tan(\alpha)\cosh^{-1}(a/r), & a_b \le r < a \\[3mm] 0 & r \ge a \end{cases}$$

$$u_r(r,0) = \begin{cases} -\dfrac{2r\tan(\alpha)}{\pi}(\dfrac{\pi a}{2}-a_b)\cdot\dfrac{1}{a+\sqrt{a^2-r^2}}\cdot(\dfrac{1+k_2}{1+k_1}\sqrt{\dfrac{l_1}{l_2}}-1)\cdot(\dfrac{1+k_1}{k_2-k_1}), & 0 \le r < a_b \\[3mm] \dfrac{r\tan(\alpha)}{2}[\log(\dfrac{r}{a+\sqrt{a^2-r^2}})-\dfrac{a^2-a\sqrt{a^2-r^2}}{r^2}](\dfrac{1+k_2}{1+k_1}\sqrt{\dfrac{l_1}{l_2}}-1)\cdot(\dfrac{1+k_1}{k_2-k_1}),, & a_b \le r < a \\[3mm] -\dfrac{a^2\tan(\alpha)}{2r}(\dfrac{1+k_2}{1+k_1}\sqrt{\dfrac{l_1}{l_2}}-1)\cdot(\dfrac{1+k_1}{k_2-k_1}), & r \ge a \end{cases}$$

$$u_z(r,0) = \begin{cases} (\dfrac{\pi a}{2}-a_b)\tan(\alpha), & 0 \le r < a_b \\[3mm] (\dfrac{\pi a}{2}-r)\tan(\alpha), & a_b \le r < a \\[3mm] a\tan(\alpha)[\sin^{-1}(\dfrac{a}{r})+\sqrt{\dfrac{r^2}{a^2}-1}-\dfrac{r}{a}], & r \ge a \end{cases}$$

$$P = P_1 + P_2$$
$$= \frac{4D(1+k_1)}{k_2-k_1}\tan(\alpha)(\frac{\pi a}{2}-a_b)(a-\sqrt{a^2-a_b^2})$$
$$-\frac{\pi D\tan(\alpha)(1+k_1)}{k_2-k_1}[a\sqrt{a^2-a_b^2}-a_b^2\cosh^{-1}(\frac{a}{a_b})]$$

2.2.2 Stress Method

When Eq.(2.12) or (2.13b) has two identical real roots, the displacement method that introduces two potential functions ϕ_1 and ϕ_2 can no longer be used. However, the stress method can be employed in this case. Ding et al. [16] elaborate the stress method for transversely isotropic material in term of one potential function in a general context. However, the stress method has not been applied to the contact problem under consideration. By using the stress method and the Hankel transforms, the normal stress, radial displacement, normal displacement and total force are derived in this section. In this method, the displacement and stress components are given by Ding et al.[16] ,

$$u_r^{II} = \frac{-e(s_{11}-s_{12})(d-mn)}{d} \frac{\partial^2 \varphi}{\partial r \partial z} , \qquad\qquad (2.42 \text{ a-f})$$

$$u_z^{II} = \frac{e(s_{11}-s_{12})(d-mn)}{d} \frac{\partial^2 \varphi}{\partial z^2} + s_{44}(\nabla_1^2 + m\frac{\partial^2}{\partial z^2})\varphi ,$$

$$\sigma_{rr}^{II} = -\frac{\partial}{\partial z}(\frac{\partial^2}{\partial r^2} + b\frac{\partial}{r\partial r} + m\frac{\partial^2}{\partial z^2})\varphi ,$$

$$\sigma_{\theta\theta}^{II} = -\frac{\partial}{\partial z}(b\frac{\partial^2}{\partial r^2} + \frac{\partial}{r\partial r} + m\frac{\partial^2}{\partial z^2})\varphi ,$$

$$\sigma_{zz}^{II} = \frac{\partial}{\partial z}(n\nabla_1^2 + d\frac{\partial^2}{\partial z^2})\varphi ,$$

$$\sigma_{zr}^{II} = \frac{\partial}{\partial r}(\nabla_1^2 + m\frac{\partial^2}{\partial z^2})\varphi$$

where s_{ij} are the components of the elastic compliance matrix ,

$$m = s_{13}(s_{11} - s_{12})/(s_{11}s_{33} - s_{13}^2), \tag{2.43 a-g}$$

$$n = [s_{11}s_{44} + s_{13}(s_{11} - s_{12})]/(s_{11}s_{33} - s_{13}^2),$$

$$d = (s_{11}^2 - s_{12}^2)/(s_{11}s_{33} - s_{13}^2),$$

$$f = s_{13}(s_{11} + s_{12})/(s_{11}s_{33} - s_{13}^2),$$

$$g = s_{11}(s_{11} + s_{12})/[2(s_{11}s_{33} - s_{13}^2)],$$

$$d - 4g + 2ge = 0,$$

$$b = 1 - e(d - mn)$$

And φ is potential function satisfying

$$(\nabla_1^2 + l_1 \frac{\partial^2}{\partial z^2})(\nabla_1^2 + l_2 \frac{\partial^2}{\partial z^2})\varphi = 0 \tag{2.44a}$$

where

$$\nabla_1^2 = \frac{\partial^2}{\partial r^2} + \frac{1}{r}\frac{\partial}{\partial r} \tag{2.44b}$$

Consider φ of the following form given by the Hankel transform:

$$\varphi = \int_0^\infty \xi R(\xi z) J_0(\xi r) d\xi \tag{2.45}$$

where $R(\xi z)$ is a function yet unknown. Using Eq. (2.45) in Eq.(2.44a) gives

$$R(\xi z) = B_1 e^{\frac{-\xi z}{\sqrt{l_1}}} + B_2 e^{\frac{-\xi z}{\sqrt{l_2}}} \tag{2.46}$$

inserting Eqs. (2.45) into Eq.(2.42a,b,e,f) gives the following stress and displacements

expressions as

$$u_r^{II} = \frac{e(s_{11} - s_{12})(d - mn)}{d} \int_0^\infty \xi^2 \frac{\partial R}{\partial z} J_1(\xi r) d\xi , \qquad (2.47\text{a-d})$$

$$u_z^{II} = \int_0^\infty \xi [\frac{e(s_{11} - s_{12})(d - mn)}{d} \frac{\partial^2 R}{\partial z^2} - s_{44} R \xi^2 + s_{44} m \frac{\partial^2 R}{\partial z^2}] J_0(\xi r) d\xi ,$$

$$\sigma_{zz}^{II} = \int_0^\infty \xi (d \frac{\partial^3 R}{\partial z^3} - n \frac{\partial R}{\partial z} \xi^2) J_0(\xi r) d\xi ,$$

$$\sigma_{zr}^{II} = \int_0^\infty \xi^2 (\xi^2 R - m \frac{\partial^2 R}{\partial z^2}) J_1(\xi r) d\xi$$

using Eqs.(2.47d) and Eq.(2.46) in Eq.(2.1b) yields

$$\sigma_{zr}^{II}(r,0) = \int_0^\infty \xi^4 (\frac{l_1 l_2 B_1 + l_1 l_2 B_2 - m l_2 B_1 - m l_1 B_2}{l_1 l_2}) J_1(\xi r) d\xi = 0 \qquad (2.48)$$

This is satisfied when

$$\frac{l_1 l_2 B_1 + l_1 l_2 B_2 - m l_2 B_1 - m l_1 B_2}{l_1 l_2} = 0 \qquad (2.49)$$

which gives

$$B_1 = \frac{m l_1 - l_1 l_2}{l_1 l_2 - m l_2} B_2 \qquad (2.50)$$

FromEqs. (2.47c) and (2.1a),it follows that

$$\sigma_{zz}^{II}(r,0) = -\int_0^\infty \xi^4 M B_2 J_0(\xi r) d\xi = 0 , \qquad (2.51 \text{ a,b})$$

$$u_z^{II}(r,0) = \int_0^\infty \xi^3 N B_2 J_0(\xi r) d\xi$$

where

$$M = \frac{-l_2^{3/2} d + \sqrt{l_2} md + n l_1 l_2^{3/2} - \sqrt{l_2} n l_1 m + l_1^{3/2} d - \sqrt{l_1} md - n l_2 l_1^{3/2} + \sqrt{l_1} n l_2 m}{l_2^{3/2} \sqrt{l_1} (l_1 - m)} , \qquad (2.52 \text{ a,b})$$

$$N = \frac{e(s_{11} - s_{12})(d - mn)(l_1 - l_2)}{dl_2(l_1 - m)}$$

Let

$$-\frac{u_z^{II}(r,0)M}{Na} = g^{II}(\tau) \tag{2.53a,b}$$

$$-\frac{Mp^3 B_2}{a^5} = F^{II}(p)$$

Then Eqs.(2.51a,b) become, with the use of Eq. (2.53a,b),

$$\int_0^\infty F^{II}(p)J_0(p\tau)dp = g^{II}(\tau), 0 < \tau < 1 \tag{2.54a,b}$$

$$\int_0^\infty pF^{II}(p)J_0(p\tau)dp = 0, \tau > 1$$

Eqs.(2.54a,b) have the same form as those of Eqs.(2.29). Hence, its solution is

also given by Eq.(2.30), with $g(y)$ defined in Eq.(2.55).

When $a_b \le r < a$, or $\dfrac{a_b}{a} \le \tau < 1$, Eqs.(2.1c) and (2.2b) can be combined to get the

normal displacement ,

$$u_z^{II}(r,0) = \delta^{II} - f(r) = \delta^{II} - (r - a_b)\tan(\alpha) \tag{2.55a}$$

using Eq.(2.54) in Eq.(2.53a)

$$g^{II}(\tau) = -\frac{[\delta^{II} - (a\tau - a_b)\tan(\alpha)]M}{Na} \tag{2.55b}$$

substituting Eq.(2.55) into eq.(2.30) leads to

$$F^{II}(p) = \frac{2M}{\pi Na}[\frac{\pi a}{2p}\tan(\alpha)\sin(p) - \frac{\delta^{II}\sin(p)}{p} - \frac{a_b \tan(\alpha)\sin(p)}{p}$$
$$- \frac{\pi a \tan(\alpha)}{2p^2} + \frac{\pi a \cos(p)\tan(\alpha)}{2p^2}] \tag{2.56a}$$

The use of eq.(2.56a) in Eq.(2.54b) yields

$$
\begin{aligned}
\sigma_{zz}^{II}(r,0) &= \int_0^\infty pF^{II}(p)J_0(p\tau)dp \\
&= \frac{2M}{\pi a N}\int_0^\infty [\sin(p)(\frac{\pi a \tan(\alpha)}{2} - \delta^{II} - a_b \tan(\alpha)]J_0(p\tau) \\
&\qquad + \int_0^\infty \frac{\pi a \tan(\alpha)}{2}(\frac{\cos(p)-1}{p})J_0(p\tau)dp
\end{aligned}
$$

(2.56b)

which requires

$$
\delta^{II} = (\frac{\pi a}{2} - a_b)\tan(\alpha)
$$

(2.56c)

inserting Eq.(2.56c) into Eq.(2.56a) then results in

$$
F^{II}(p) = \frac{M\tan(\alpha)[\cos(p)-1]}{Np^2}
$$

(2.56d)

From Eq.(2.53b), it follows that

$$
\begin{aligned}
B_2 &= -\frac{F^{II}(p)a^5}{Mp^3} \\
&= -\frac{2a^4}{\pi Np^3}[\frac{\pi a}{2p}\tan(\alpha)\sin(p) - \frac{\delta^{II}\sin(p)}{p} - \frac{a_b\tan(\alpha)\sin(p)}{p} \\
&\qquad - \frac{\pi a\tan(\alpha)}{2p^2} + \frac{\pi a\cos(p)\tan(\alpha)}{2p^2}]
\end{aligned}
$$

(2.56e)

using Eqs.(2.46),(2.50),(2.56e),(2.52) in Eqs.(2.47 a,b,c) finally gives

$$
\sigma_{zz}^{II}(r,0) = -\frac{M}{N}\tan(\alpha)\cosh^{-1}(\frac{a}{r}), \qquad a_b \le r < a
$$

(2.57a-d)

$$u_r^{II}(r,0) = -\frac{Qa}{M}\int_0^\infty F^{II}(p)J_1(p\tau)dp$$

$$= \begin{cases} -\dfrac{Q\tan(\alpha)}{2N}r[\log(\dfrac{r}{a+\sqrt{a^2-r^2}}) - \dfrac{a^2-a\sqrt{a^2-r^2}}{r^2}], & a_b \le r < a \\[4mm] \dfrac{Qa^2\tan(\alpha)}{2Nr}, & r \ge a \end{cases}$$

$$u_z^{II}(r,0) = \begin{cases} (\dfrac{\pi a}{2} - r)\tan(\alpha), & a_b \le r < a \\[4mm] a\tan(\alpha)[\sin^{-1}(\dfrac{a}{r}) + \sqrt{\dfrac{r^2}{a^2}-1} - \dfrac{r}{a}], & r \ge a \end{cases}$$

$$P_1^{II} = \frac{\pi M}{N}\tan(\alpha)[a\sqrt{a^2-a_b^2} - a_b^2\cosh^{-1}(\frac{a}{a_b})], \quad a_b \le r < a$$

where,

$$Q = \frac{e(s_{11}-s_{12})(d-mn)}{d}[\frac{\sqrt{l_1}(l_2-m)}{l_2(l_1-m)} - \frac{1}{\sqrt{l_2}}] \tag{2.58}$$

Similarly, for the region $0 \le r < a_b$, or $0 \le \tau < \dfrac{a_b}{a}$, it can be shown that

$$u_z^{II}(r,0) = \delta^{II} = (\frac{\pi a}{2} - a_b)\tan(\alpha), \tag{2.59a-g}$$

$$g^{II}(\tau) = -\frac{M}{Na}(\frac{\pi a}{2} - a_b)\tan(\alpha),$$

$$F^{II}(p) = -\frac{2M}{\pi Na}(\frac{\pi a}{2} - a_b)\tan(\alpha)\frac{\sin(p)}{p}$$

$$\sigma_{zz}^{II}(r,0) = -\frac{2M}{\pi N}(\frac{\pi a}{2} - a_b)\tan(\alpha)\frac{1}{\sqrt{a^2-r^2}} \qquad 0 \le r < a_b$$

$$u_r^{II}(r,0) = -\frac{Qa}{M}\int_0^\infty F^{II}(p)J_1(p\tau)dp$$

$$= \frac{2Qr}{\pi N}(\frac{\pi a}{2}-a_b)\tan(\alpha)\cdot\frac{1}{a+\sqrt{a^2-r^2}}, \qquad 0\le r < a_b$$

$$u_z^{II}(r,0) = (\frac{\pi a}{2}-a_b)\tan(\alpha), \qquad 0\le r < a_b$$

$$P_2^{II} = \frac{4M}{N}(\frac{\pi a}{2}-a_b)\tan(\alpha)(a-\sqrt{a^2-a_b^2}), \ \ 0\le r < a_b$$

Thus, combining Eqs. (2.57) and (2.59) results in

$$\delta^{II} = (\frac{\pi a}{2}-a_b)\tan(\alpha) \hspace{5cm} (2.60\text{a-e})$$

$$\sigma_{zz}^{II}(r,0) = \begin{cases} -\dfrac{2M}{\pi N}(\dfrac{\pi a}{2}-a_b)\tan(\alpha)\dfrac{1}{\sqrt{a^2-r^2}} & 0\le r < a_b \\[3mm] -\dfrac{M}{N}\tan(\alpha)\cosh^{-1}(\dfrac{a}{r}) & a_b \le r < a \\[3mm] 0 & r\ge a \end{cases}$$

$$u_r^{II}(r,0) = \begin{cases} \dfrac{2Qr}{\pi N}(\dfrac{\pi a}{2}-a_b)\tan(\alpha)\cdot\dfrac{1}{a+\sqrt{a^2-r^2}}, & 0\le r < a_b \\[3mm] -\dfrac{Q\tan(\alpha)}{2N}r[\log(\dfrac{r}{a+\sqrt{a^2-r^2}})-\dfrac{a^2-a\sqrt{a^2-r^2}}{r^2}], & a_b \le r < a \\[3mm] \dfrac{Qa^2\tan(\alpha)}{2Nr}, & r\ge a \end{cases}$$

$$u_z^{II}(r,0) = \begin{cases} (\dfrac{\pi a}{2}-a_b)\tan(\alpha) & \\[3mm] (\dfrac{\pi a}{2}-r)\tan(\alpha), & a_b \le r < a \\[3mm] a\tan(\alpha)[\sin^{-1}(\dfrac{a}{r})+\sqrt{\dfrac{r^2}{a^2}-1}-\dfrac{r}{a}], & r\ge a \end{cases}$$

$$P^{II} = P_1^{II} + P_2^{II}$$

$$= \frac{4M}{N}(\frac{\pi a}{2} - a_b)\tan(\alpha)(a - \sqrt{a^2 - a_b^2})$$

$$+ \frac{\pi M}{N}\tan(\alpha)[a\sqrt{a^2 - a_b^2} - a_b^2\cosh^{-1}(\frac{a}{a_b})]$$

These are valid when Eq.(2.12) or Eq.(2.13b) has two identical real roots.

2.3. The Boussinesq Contact of a Cylindrical Punch

The adhesive contact can be viewed as a superposition of the Hertz contact and the Boussinesq contact (Chen and Yu [17]). Thus, it is necessary to introduce the Boussinesq contact in this section.

2.3.1 An Axisymmetric External Crack in an Infinite Body

Consider the problem of an axisymmetric external crack in an infinite elastic body of an transversely isotropic material as shown in Fig.2.3.
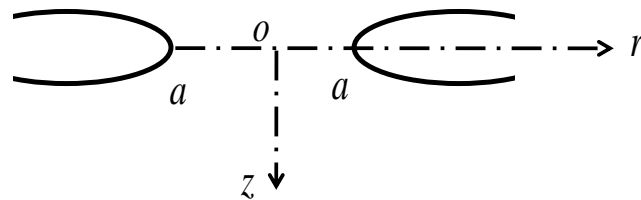

Fig.2.3 Axisymmetric external crack problem

Due to the symmetry, only a semi-infinite space $z \geq 0$ needs to be considered. The boundary conditions for this crack problem are given by(Chen and Yu [17])

$$u_z^\Theta(r,0)=0, \qquad 0 \le r \le a \tag{2.61a-c}$$

$$\sigma_{zz}^\Theta(r,0)=-h(r), \quad r>a$$

$$\sigma_{zr}^\Theta(r,0)=0, \qquad r \ge 0$$

The governing equations are the same as those given in Eq.(2.7a,b). Using a similar approach to that employed in Section 2.2.1, the following dual integral equations can be obtained

$$\int_0^\infty \psi(p)J_0(p\tau)dp=-h(r), \qquad \tau>1 \tag{2.62 a,b}$$

$$\int_0^\infty p^{-1}\psi(p)J_0(p\tau)dp=0, \quad 0<\tau<1$$

where

$$\psi(p)=\frac{p^3}{a^4}\frac{1}{\sqrt{l_2}}DA(\xi) \tag{2.63}$$

Lowengrub and Sneddon[18] discussed how to solve this pair of dual integral equations. Especially, for a constant pressure distribution $h(r)=h_0$ on the crack surface region $a \le r \le c$, it can be shown that (Maguies,1992[6])

$$\sigma_{zz}^\Theta(r,0)=\frac{2h_0}{\pi}[\sqrt{\frac{c^2-a^2}{a^2-r^2}}-\tan^{-1}(\sqrt{\frac{c^2-a^2}{a^2-r^2}})].(0 \le r \le a) \tag{2.64}$$

Then, the total axial force acting on the neck region is given by

$$P^\Theta=2\pi\int_0^a r\sigma_{zz}^\Theta dr=h_0\pi(c^2-a^2)-2h_0a^2[\frac{c^2}{a^2}\cos^{-1}(\frac{a}{c})-\sqrt{\frac{c^2}{a^2}-1}] \tag{2.65}$$

Clearly, Eq. (2.65) shows that the total force applied on the cylindrical punch does not equilibrate the force $h_0\pi(c^2 - a^2)$, which is acting on the external crack surface. This indicates that a compressive force exists in the neck region, which is the second term on the right hand side of Eq.(2.65).

2.3.2 The Boussinesq Contact Problem

The Boussinesq contact problem of a cylindrical punch of a radius a indenting a half space is considered. The force added on the punch is upward. It is shown in Fig.2.4.
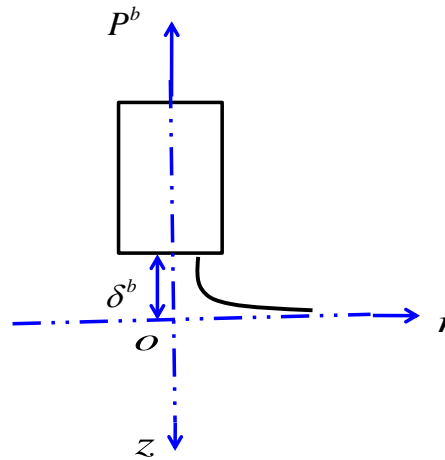

Fig.2.4 Boussinesq contact of a cylindrical punch

To consider the crack singularity, the force added on the punch is given by,

$$P^b = 2h_0 a^2 [\frac{c^2}{a^2}\cos^{-1}(\frac{a}{c}) - \sqrt{\frac{c^2}{a^2} - 1}]$$

(2.66)

By using Eq.(2.66), the depth of penetration, normal stress and vertical displacement can be calculated. For the case with two distinct real roots, the results are,

$$\delta^b = \frac{(P^H - P^b)(k_2 - k_1)}{4aD(1 + k_1)} \tag{2.67a-c}$$

$$\sigma_{zz}^b(r,0) = \frac{P^H - P^b}{2\pi a\sqrt{a^2 - r^2}}$$

$$u_z^b(r,0) = \begin{cases} \delta^b, & 0 \le r < a \\ \dfrac{2}{\pi}\delta^b \sin^{-1}(\dfrac{a}{r}), & r > a \end{cases}$$

For the case with two identical real roots, the results are,

$$\delta^b = \frac{(P^H - P^b)N}{4aM} \tag{2.68a-c}$$

$$\sigma_{zz}^b(r,0) = \frac{P^H - P^b}{2\pi a\sqrt{a^2 - r^2}}$$

$$u_z^b(r,0) = \begin{cases} \delta^b, & 0 \le r < a \\ \dfrac{2}{\pi}\delta^b \sin^{-1}(\dfrac{a}{r}), & r > a \end{cases}$$

where P^H is the total force of the Hertz contact shown in Section 2.2.

2.4. The Adhesive Contact of a Conical Frustum Punch

As mentioned before, the adhesive contact problem can be decomposed into two parts: a Hertz contact problem and a Boussinesq contact problem, as shown in Fig 2.5.
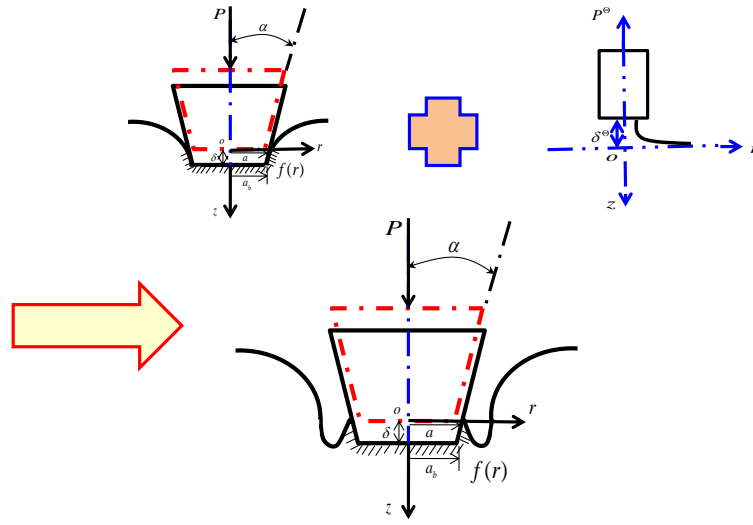
Fig. 2.5 Adhesive contact problem by the superposition principle

Combining the results obtained in Sections 2.2 and 2.3, the adhesive contact problem can be readily solved. For the case with two distinct real roots discussed in Section 2.2.1, the results are

$$
\delta^T = \tan(\alpha)(\frac{\pi a}{2} - a_b) + \frac{(k_2 - k_1)}{4aD(1+k_1)} \{ \frac{4D(1+k_1)}{k_2 - k_1} \tan(\alpha)(\frac{\pi a}{2} - a_b)(a - \sqrt{a^2 - a_b^2})
$$

$$
- \frac{\pi D \tan(\alpha)(1+k_1)}{k_2 - k_1} [a\sqrt{a^2 - a_b^2} - a_b^2 \cosh^{-1}(\frac{a}{a_b})] - 2h_0 a^2 [\frac{c^2}{a^2} \cos^{-1}(\frac{a}{c}) - \sqrt{\frac{c^2}{a^2} - 1}] \}
$$

$$
(2.69\text{a-d})
$$

$$\sigma_{zz}^{T}(r,0) = \begin{cases} -\dfrac{2D(1+k_{1})}{\pi(k_{2}-k_{1})}\tan(\alpha)(\dfrac{\pi a}{2}-a_{b})\cdot\dfrac{1}{\sqrt{a^{2}-r^{2}}} \\[2mm] \quad +\dfrac{1}{2\pi a\sqrt{a^{2}-r^{2}}}\{\dfrac{4D(1+k_{1})}{k_{2}-k_{1}}\tan(\alpha)(\dfrac{\pi a}{2}-a_{b})(a-\sqrt{a^{2}-a_{b}^{2}}) \\[2mm] \qquad -\dfrac{\pi D\tan(\alpha)(1+k_{1})}{k_{2}-k_{1}}[a\sqrt{a^{2}-a_{b}^{2}}-a_{b}^{2}\cosh^{-1}(\dfrac{a}{a_{b}})] \\[2mm] \qquad\qquad -2h_{0}a^{2}[\dfrac{c^{2}}{a^{2}}\cos^{-1}(\dfrac{a}{c})-\sqrt{\dfrac{c^{2}}{a^{2}}-1}]\}, \quad 0\le r<a_{b} \\[4mm] -\dfrac{(1+k_{1})}{k_{2}-k_{1}}D\tan(\alpha)\cosh^{-1}(a/r) \\[2mm] \quad +\dfrac{1}{2\pi a\sqrt{a^{2}-r^{2}}}\{\dfrac{4D(1+k_{1})}{k_{2}-k_{1}}\tan(\alpha)(\dfrac{\pi a}{2}-a_{b})(a-\sqrt{a^{2}-a_{b}^{2}}) \\[2mm] \qquad -\dfrac{\pi D\tan(\alpha)(1+k_{1})}{k_{2}-k_{1}}[a\sqrt{a^{2}-a_{b}^{2}}-a_{b}^{2}\cosh^{-1}(\dfrac{a}{a_{b}})] \\[2mm] \qquad\qquad -2h_{0}a^{2}[\dfrac{c^{2}}{a^{2}}\cos^{-1}(\dfrac{a}{c})-\sqrt{\dfrac{c^{2}}{a^{2}}-1}]\}, \ a_{b}\le r<a \\[4mm] 0 \qquad\qquad\qquad\qquad\qquad\qquad\qquad\qquad\qquad\quad r\ge a \end{cases}$$

$$u_{z}^{T}(r,0) = \begin{cases} (\dfrac{\pi a}{2}-a_{b})\tan(\alpha)+\dfrac{(k_{2}-k_{1})}{4aD(1+k_{1})}\{\dfrac{4D(1+k_{1})}{k_{2}-k_{1}}\tan(\alpha)(\dfrac{\pi a}{2}-a_{b})(a-\sqrt{a^{2}-a_{b}^{2}}) \\[2mm] \quad -\dfrac{\pi D\tan(\alpha)(1+k_{1})}{k_{2}-k_{1}}[a\sqrt{a^{2}-a_{b}^{2}}-a_{b}^{2}\cosh^{-1}(\dfrac{a}{a_{b}})] \\[2mm] \qquad -2h_{0}a^{2}[\dfrac{c^{2}}{a^{2}}\cos^{-1}(\dfrac{a}{c})-\sqrt{\dfrac{c^{2}}{a^{2}}-1}]\}, \quad 0\le r<a_{b} \\[4mm] (\dfrac{\pi a}{2}-r)\tan(\alpha)+\dfrac{(k_{2}-k_{1})}{4aD(1+k_{1})}\{\dfrac{4D(1+k_{1})}{k_{2}-k_{1}}\tan(\alpha)(\dfrac{\pi a}{2}-a_{b})(a-\sqrt{a^{2}-a_{b}^{2}}) \\[2mm] \quad -\dfrac{\pi D\tan(\alpha)(1+k_{1})}{k_{2}-k_{1}}[a\sqrt{a^{2}-a_{b}^{2}}-a_{b}^{2}\cosh^{-1}(\dfrac{a}{a_{b}})] \\[2mm] \qquad -2h_{0}a^{2}[\dfrac{c^{2}}{a^{2}}\cos^{-1}(\dfrac{a}{c})-\sqrt{\dfrac{c^{2}}{a^{2}}-1}]\}, \quad a_{b}\le r<a \\[4mm] a\tan(\alpha)[\sin^{-1}(\dfrac{a}{r})+\sqrt{\dfrac{r^{2}}{a^{2}}-1}-\dfrac{r}{a}] \\[2mm] \quad +\dfrac{(k_{2}-k_{1})}{2\pi aD(1+k_{1})}\{\dfrac{4D(1+k_{1})}{k_{2}-k_{1}}\tan(\alpha)(\dfrac{\pi a}{2}-a_{b})(a-\sqrt{a^{2}-a_{b}^{2}}) \\[2mm] \quad -\dfrac{\pi D\tan(\alpha)(1+k_{1})}{k_{2}-k_{1}}[a\sqrt{a^{2}-a_{b}^{2}}-a_{b}^{2}\cosh^{-1}(\dfrac{a}{a_{b}})] \\[2mm] \qquad -2h_{0}a^{2}[\dfrac{c^{2}}{a^{2}}\cos^{-1}(\dfrac{a}{c})-\sqrt{\dfrac{c^{2}}{a^{2}}-1}]\}\sin^{-1}(\dfrac{a}{r}) \quad r\ge a \end{cases}$$

$$P^T = \frac{4D(1+k_1)}{k_2 - k_1} \tan(\alpha)(\frac{\pi a}{2} - a_b)(a - \sqrt{a^2 - a_b^2})$$

$$- \frac{\pi D \tan(\alpha)(1+k_1)}{k_2 - k_1}[a\sqrt{a^2 - a_b^2} - a_b^2 \cosh^{-1}(\frac{a}{a_b})]$$

$$- 2h_0 a^2 [\frac{c^2}{a^2} \cos^{-1}(\frac{a}{c}) - \sqrt{\frac{c^2}{a^2} - 1}]$$

For the case with two identical real roots discussed in Section 2.2.2, the results are

$$\delta^T = \tan(\alpha)(\frac{\pi a}{2} - a_b) + \frac{N}{4aM}\{\frac{4M}{N}(\frac{\pi a}{2} - a_b)\tan(\alpha)(a - \sqrt{a^2 - a_b^2})$$

$$+ \frac{\pi M}{N}\tan(\alpha)[a\sqrt{a^2 - a_b^2} - a_b^2 \cosh^{-1}(\frac{a}{a_b})] - 2h_0 a^2 [\frac{c^2}{a^2} \cos^{-1}(\frac{a}{c}) - \sqrt{\frac{c^2}{a^2} - 1}]\}$$

$$(2.70\text{a-d})$$

$$\sigma_{zz}^T(r,0) = \begin{cases} \begin{aligned} &-\frac{2M}{\pi N}\tan(\alpha)(\frac{\pi a}{2} - a_b) \cdot \frac{1}{\sqrt{a^2 - r^2}} \\ &\quad + \frac{1}{2\pi a\sqrt{a^2 - r^2}}\{\frac{4M}{N}(\frac{\pi a}{2} - a_b)\tan(\alpha)(a - \sqrt{a^2 - a_b^2}) \\ &\quad + \frac{\pi M}{N}\tan(\alpha)[a\sqrt{a^2 - a_b^2} - a_b^2 \cosh^{-1}(\frac{a}{a_b})] - 2h_0 a^2[\frac{c^2}{a^2}\cos^{-1}(\frac{a}{c}) - \sqrt{\frac{c^2}{a^2} - 1}]\}, \quad 0 \le r < a_b \\ &-\frac{M}{N}D\tan(\alpha)\cosh^{-1}(a/r) + \frac{1}{2\pi a\sqrt{a^2 - r^2}}\{\frac{4M}{N}(\frac{\pi a}{2} - a_b)\tan(\alpha)(a - \sqrt{a^2 - a_b^2}) \\ &\quad + \frac{\pi M}{N}\tan(\alpha)[a\sqrt{a^2 - a_b^2} - a_b^2 \cosh^{-1}(\frac{a}{a_b})] - 2h_0 a^2[\frac{c^2}{a^2}\cos^{-1}(\frac{a}{c}) - \sqrt{\frac{c^2}{a^2} - 1}]\} \quad a_b \le r < a \\ &0 \qquad\qquad\qquad\qquad\qquad\qquad\qquad\qquad\qquad\qquad\qquad\qquad\qquad\qquad r \ge a \end{aligned} \end{cases}$$

$$u_z^T(r,0) = \begin{cases} (\dfrac{\pi a}{2} - a_b)\tan(\alpha) + \dfrac{N}{4aM}\{\dfrac{4M}{N}(\dfrac{\pi a}{2} - a_b)\tan(\alpha)(a - \sqrt{a^2 - a_b^2}) \\ \quad + \dfrac{\pi M}{N}\tan(\alpha)[a\sqrt{a^2 - a_b^2} - a_b^2\cosh^{-1}(\dfrac{a}{a_b})] \\ \quad\quad - 2h_0a^2[\dfrac{c^2}{a^2}\cos^{-1}(\dfrac{a}{c}) - \sqrt{\dfrac{c^2}{a^2} - 1}]\}, \quad 0 \le r < a_b \\[2ex] (\dfrac{\pi a}{2} - r)\tan(\alpha) + \dfrac{N}{4aM}\{\dfrac{4M}{N}(\dfrac{\pi a}{2} - a_b)\tan(\alpha)(a - \sqrt{a^2 - a_b^2}) \\ \quad + \dfrac{\pi M}{N}\tan(\alpha)[a\sqrt{a^2 - a_b^2} - a_b^2\cosh^{-1}(\dfrac{a}{a_b})] \\ \quad\quad - 2h_0a^2[\dfrac{c^2}{a^2}\cos^{-1}(\dfrac{a}{c}) - \sqrt{\dfrac{c^2}{a^2} - 1}]\}, \quad a_b \le r < a \\[2ex] a\tan(\alpha)[\sin^{-1}(\dfrac{a}{r}) + \sqrt{\dfrac{r^2}{a^2} - 1} - \dfrac{r}{a}] + \dfrac{N}{2\pi aM}\{\dfrac{4M}{N}(\dfrac{\pi a}{2} - a_b)\tan(\alpha)(a - \sqrt{a^2 - a_b^2}) \\ \quad + \dfrac{\pi M}{N}\tan(\alpha)[a\sqrt{a^2 - a_b^2} - a_b^2\cosh^{-1}(\dfrac{a}{a_b})] \\ \quad\quad - 2h_0a^2[\dfrac{c^2}{a^2}\cos^{-1}(\dfrac{a}{c}) - \sqrt{\dfrac{c^2}{a^2} - 1}]\}\sin^{-1}(\dfrac{a}{r}), \quad r \ge a \end{cases}$$

$$P^T = \dfrac{4M}{N}(\dfrac{\pi a}{2} - a_b)\tan(\alpha)(a - \sqrt{a^2 - a_b^2})$$
$$+ \dfrac{\pi M}{N}\tan(\alpha)[a\sqrt{a^2 - a_b^2} - a_b^2\cosh^{-1}(\dfrac{a}{a_b})] - 2h_0a^2[\dfrac{c^2}{a^2}\cos^{-1}(\dfrac{a}{c}) - \sqrt{\dfrac{c^2}{a^2} - 1}]$$

2.5. The Numerical Results for the Adhesive Contact Problem

For numerical analysis, the selected transversely isotropic material and elastic constants values are shown in Table 2.1.

Penetration depth, normal stress, normal displacement and total force are studied by comparing the adhesive contact and the Hertz contact. Especially for adhesive contact, different values for h_0 are set for the results from both displacement and stress methods. They are 0.1GPa, 0.5GPa, 1GPa and 1.5GPa, respectively. The ratio values for

a/c and a_b/a are prescribed as 0.2 for each case studied. The punch angle α=30deg is chosen.

Table 2.1 The selected transversely isotropic material and elastic constants

Transversely Isotropic Masterial		Graphite/Expoxy Composite						
Displacement Method (M1)	Stiffness Matrix Components (Gpa)	c_{11}	c_{12}	c_{13}	c_{33}	c_{44}	Refer to [19]	
		8.28	2.767	0.285	86.8	4.147		
	Other Used Values in M1	k_1	k_2	v_1	v_2	D (10^{10})	By eqns (2.13), (2.14) & (2.26)	
		37.44	0.027	20.54	0.52	-2.23		
Stress Method (M2)	Compliance Matrix Components (10^{-10})	s_{11}	s_{12}	s_{13}	s_{22}	s_{33}	s_{44}	s_{66}
		1.36	-0.454	-0.003	1.36	0.115	1.21	1.81
	Other Used Values in M2	m	n	d	f	g	e	b
		-0.034	10.429	10.483	-0.017	3.929	0.666	-6.219
		M	N (10^{-10})	l_1	l_2	By eqns (2.44) & (2.55)		
		-22.630	0.963	9.261	1.134			

Figures 2.6 and 2.7 show the penetration depth of the conical frustum punch versus contact radius comparisons for each case from displacement and stress methods. Clearly seen from both methods, the penetration depth increases as the contact radius increases and the results from adhesive contact are upper bounded by Hertz contact. Especially when h_0=0.1GPa, the adhesive contact and the Hertz contact have no large difference. As h_0 varies from 0.1 GPa to 1.5 GPa, if given the same contact radius, the

penetration depth decreased faster for displacement method, compared with the results
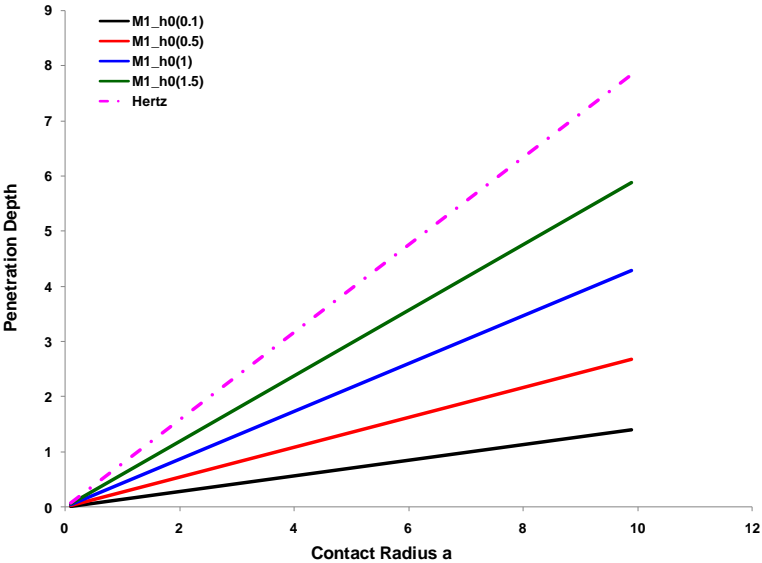
from the stress method.

Fig. 2.6 Penetration depth of the conical frustum punch versus contact radius comparisons for displacement method
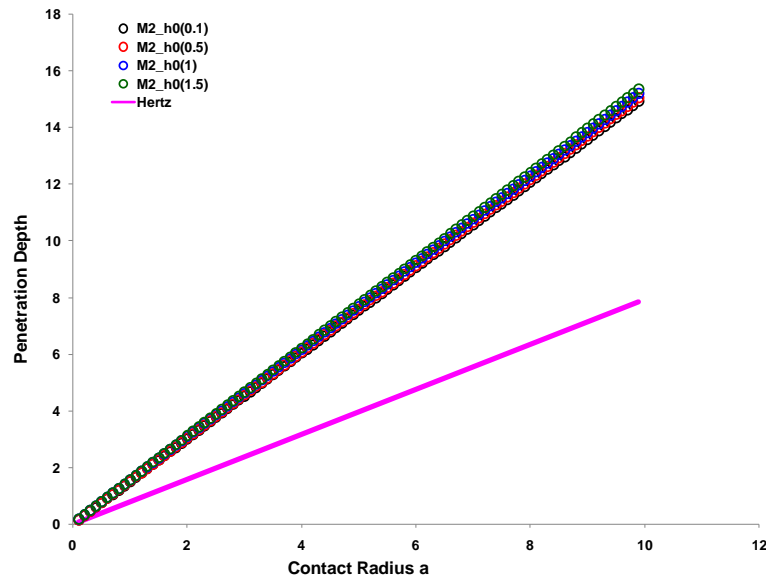
Fig. 2.7 Penetration depth of the conical frustum punch versus contact radius comparisons for stress method

Figures 2.8 and 2.9 reveal the normal stress on the plane *z=0* versus *r/a* ratio comparisons for both displacement and stress methods. When *r/a<1*, the region studied is inside the contact region.

For both displacement and stress methods, inside the contact zone, the negative normal stress arises smoothly as the *r/a* ratio increases but with different directions. When *r/a=0.3*, the negative normal stress values approach the peak values. Once *r/a>0.3*, the negative normal stress would go down suddenly in the cohesive zone. After *r/a* is larger than around 0.9, the normal stress values tend increasing. As *h₀* varies from 0.1 GPa to 1.5 GPa, given the same *r/a* ratio value, the negative normal stress values increases for both methods. Also, the four cases for adhesive contact are lower bounded by the Hertz contact for both methods. For the zones inside the circle shown in Figs 2.8 and 2.9, the adhesive contact results change more gently than the Hertz contact, which is

caused by the Boussinesq contact assuming the peeling upwards force inside the cohesive region.
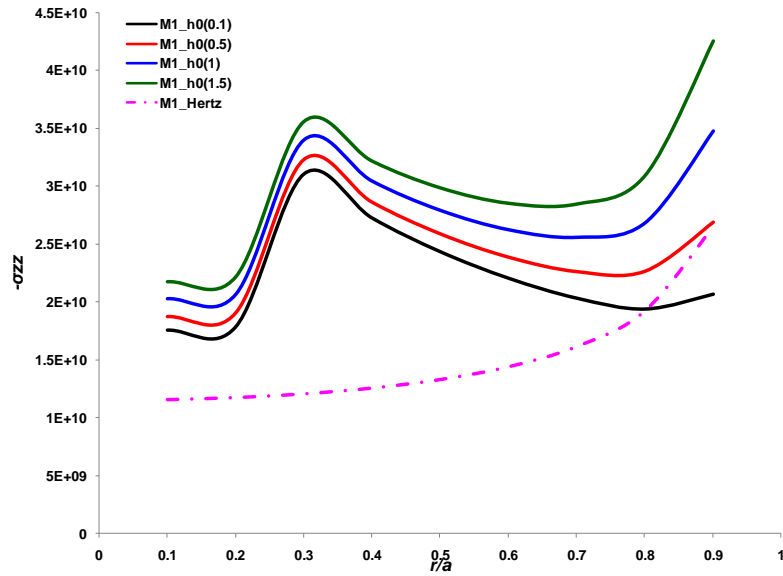

Fig. 2.8 Normal stress on the plane $z=0$ versus r/a ratio comparisons for displacement method
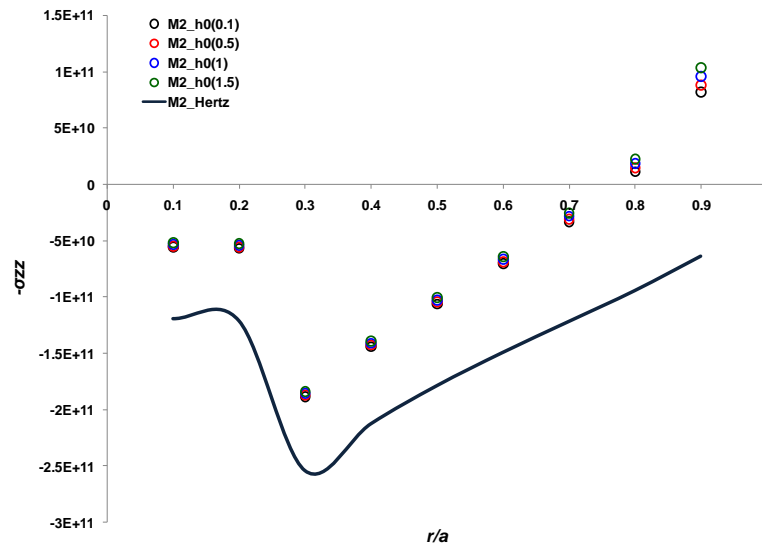

Fig. 2.9 Normal stress on the plane $z=0$ versus r/a ratio comparisons for stress method

Figures 2.10 and 2.11 indicate the normal displacement the plane $z=0$ changes with r/a ratio for both displacement and stress methods. Seen from both figures, inside the circle zones, the negative normal displacement values keep constant firstly and then increase sharply. Before $r/a=0.2$, it is the punch flat-end part. The normal displacements are the same for all the points along the flat end. For $0.2<r/a<5$, the negative normal displacement goes up for each case and reaches the peak values at $r/a =5$. As h_0 varies from 0.1 GPa to 1.5 GPa, given the same r/a ratio value, the negative normal displacement values increase and the adhesive contact results are lower bounded by the Hertz contact results for both methods. The intervals between each case in displacement method are larger than the stress method.
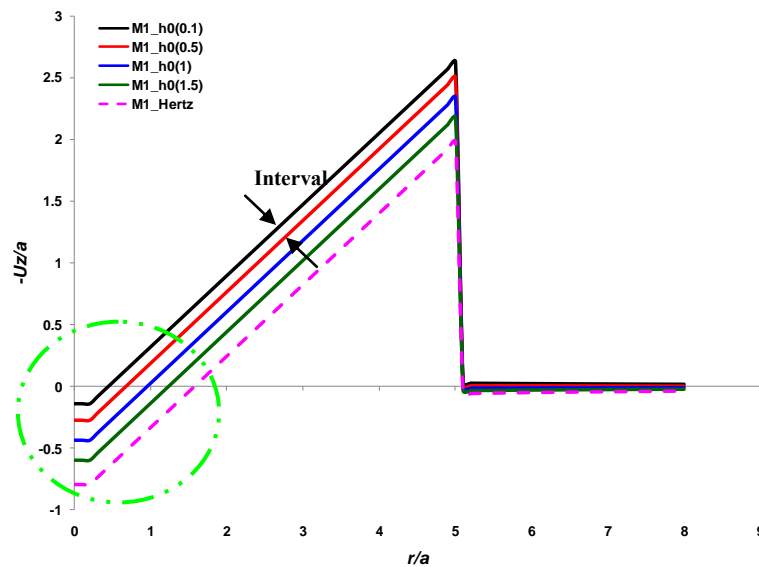

Fig. 2.10 Normal displacement on the plane $z=0$ versus r/a ratio comparisons for displacement method
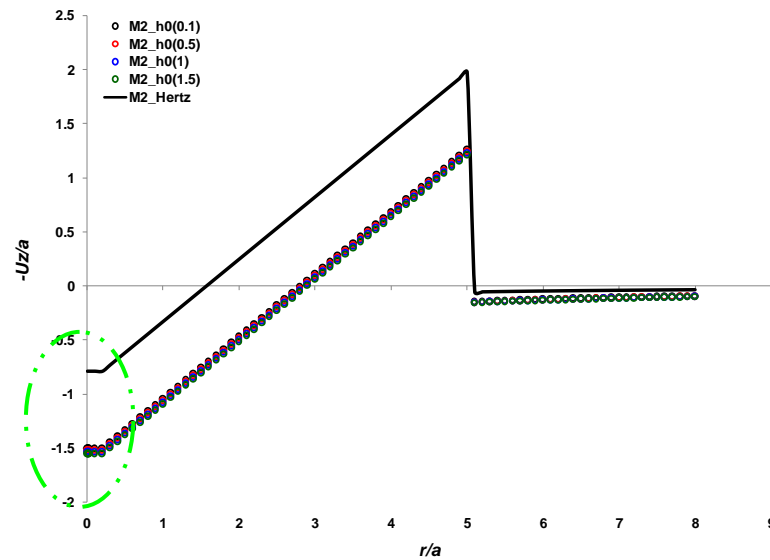
Fig. 2.11 Normal displacement on the plane *z*=0 versus *r/a* ratio comparisons for stress method

Figure 2.12 shows the total force added on the punch versus the contact radius for the displacement method. Clearly, with contact radius increasing, the total force increases in the negative direction. When h_0 changes from 0.1 GPa to 1.5GPa, the direction of the total force is never changed. Compared with the Fig.2.12, Figure 2.13 shows the total force increases with the contact area for the stress method. However, for different cases, the influence of h_0 is different. The displacement method is affected significantly by h_0 while the stress method is affected less.

Fig. 2.12 Total force of the conical frustum punch versus contact radius comparisons for displacement method

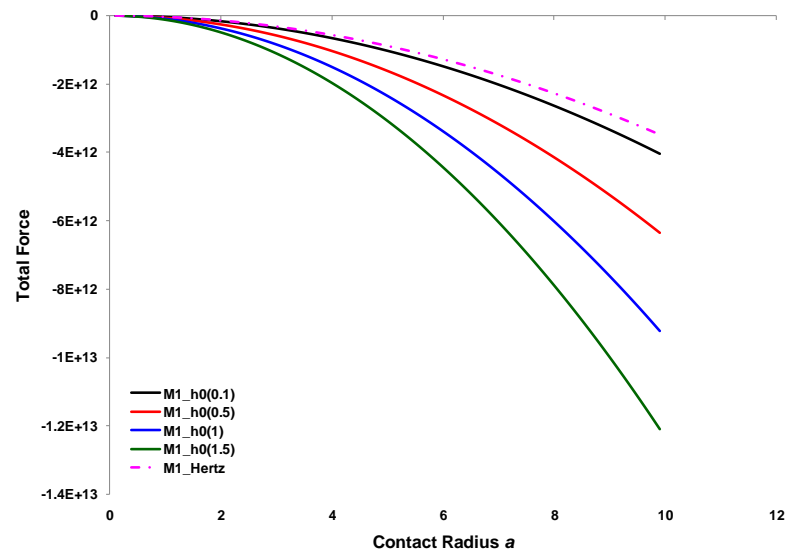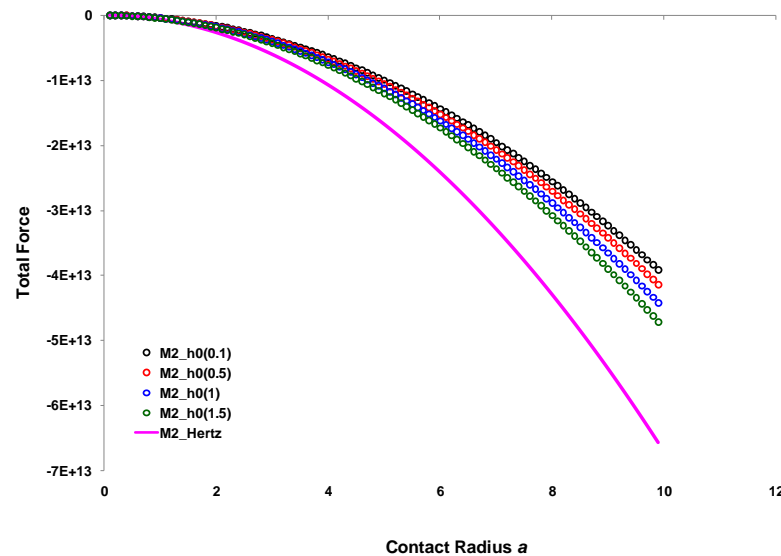**Fig. 2.13 Total force of the conical frustum punch versus contact radius comparisons for stress method**

Figure 2.14 shows the total force added on the punch versus the penetration depth for the displacement method. Clearly, with contact radius increasing, the total

force increases. When h_0 changes from 0.1 GPa to 1.5GPa, the changes of the total force

become more smoothly. Compared with the Fig.2.14, Figure 2.15 shows the total force

increases with the penetration depth for the stress method. However, for different cases,

the influence of h_0 is different. The displacement method is affected significantly by h_0

while the stress method is affected less. They are both upper bounded by Hertz contact.
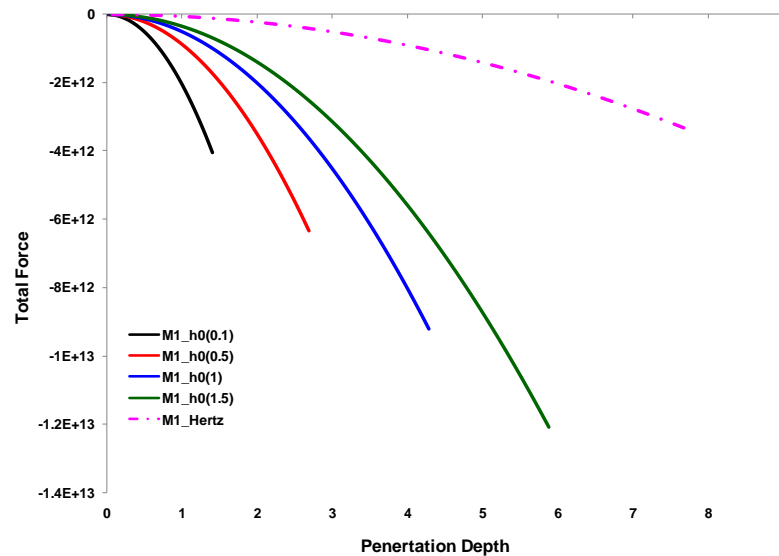
Fig. 2.14 Total force of the conical frustum punch versus penetration depth comparisons for displacement method
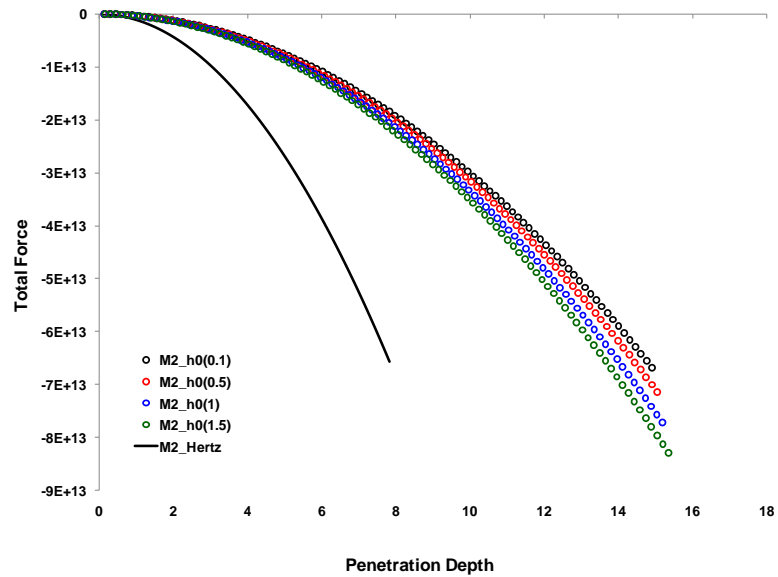
Fig. 2.15 Total force of the conical frustum punch versus penetration depth comparisons for stress method

The stress method can be used to solve the indentation problem for isotropic material and Eqs. (2.71) can be reduced. If a_b is set zero, a solution of the adhesive contact problem of a rigid conical punch with an isotropic half space can be obtained. The selected isotropic material is listed in Table 2.2. The numerical analysis results are compared with the ones shown in Maguis and Barguins [20] by using the JKR adhesive contact model. The difference between the JKR and MD adhesive contact models are clearly shown.

Table 2.2 The selected isotropic material and elastic moduli values

Isotropic Material							
Aluminum	E (Gpa)	v	μ (Gpa)	λ (Gpa)	k (Gpa)	By eqns (2.44) & (2.55)	
	68.9	0.34	25.700	54.6	71.8	Refer to [21]	
Compliance Matrix Components	S_{11} (10^{-12})	S_{12} (10^{-12})	S_{13} (10^{-12})	S_{33} (10^{-12})	S_{44} (10^{-12})	M	N (10^{-10})
	14.514	-4.935	-4.935	14.51	19.448	2	-1.05
Other Used Values	m	n	d	f	g	e	b
	-0.515	1.000	1.000	-0.254	-0.724	2.69	-3.076

Figures 2.16-2.18 compare the JKR and the MD adhesive contact models with different pressure constant h_0 and energy of adhesion w values which are set at 0.01 GPa, 0.1 GPa and 1GPa, respectively. The penetration depth increases as the contact radius increases. Especially at 0.01 GPa, the JKR adhesive contact model is essentially coincident with the MD adhesive contact model. With pressure constant h_0 and energy of adhesion w values changing from 0.01 GPa to 1 GPa, the difference between these two adhesive contact models becomes larger. Thus, for this selected isotropic material, there is a transition between these two adhesive contact models and when the adhesive interaction is prescribed as a small value, the MD adhesive contact model can approach the results as the JKR model.
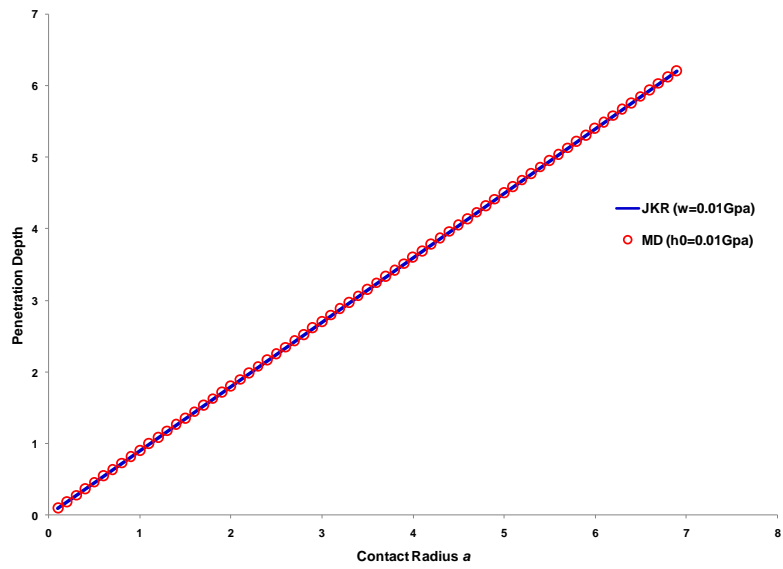
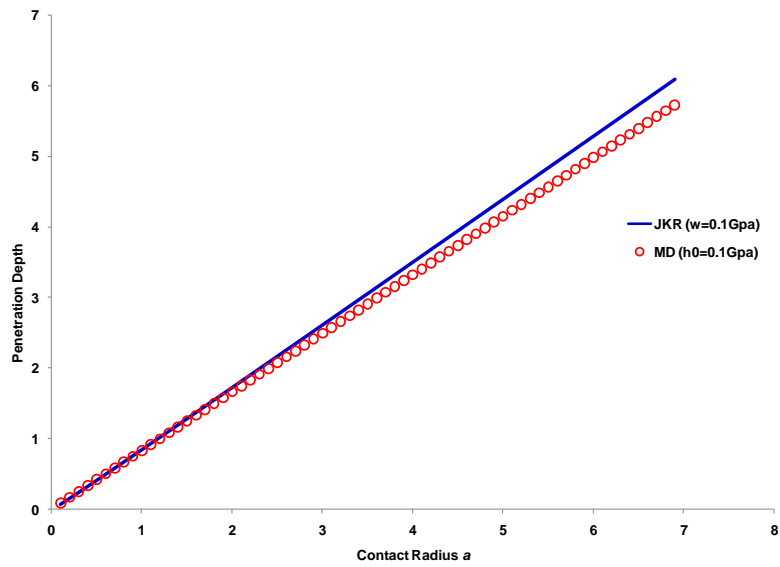**Fig. 2.16 Penetration depth versus contact radius for both the JKR and the MD models (w=h0=0.01 GPa)**

Fig. 2.17 Penetration depth versus contact radius for both the JKR and the MD models (w=h0=0.1 GPa)
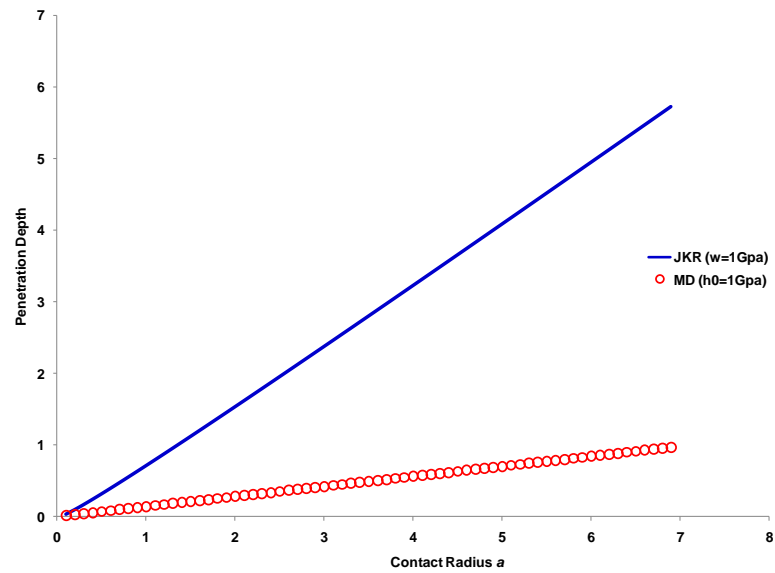
Fig. 2.18 Penetration depth versus contact radius for both the JKR and the MD models (w=h0=1 GPa)

Figures 2.19-2.21 show the contact radius changes with the total force added on the conical punch indenting an isotropic half space. With different pressure constant h_0 and energy of adhesion w values, as the total force arises, the contact radius increases. As the constant values increase from 0.01 GPa to 1 GPa, the increasing tendency becomes gentle. Given the same external force, the JKR adhesive contact model can achieve a larger contact radius compared with the MD adhesive contact model. This is identical with the results in Zhang [22]. As the adhesive interaction becomes bigger, to reach the same contact radius, a larger external force needs to be added on the conical punch.
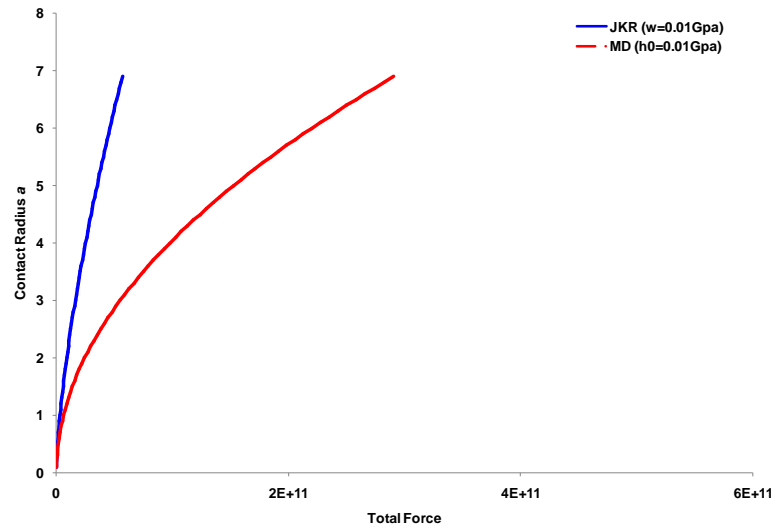
Fig. 2.19 Contact radius versus total force for both the JKR and the MD models (w=h0=0.01 GPa)
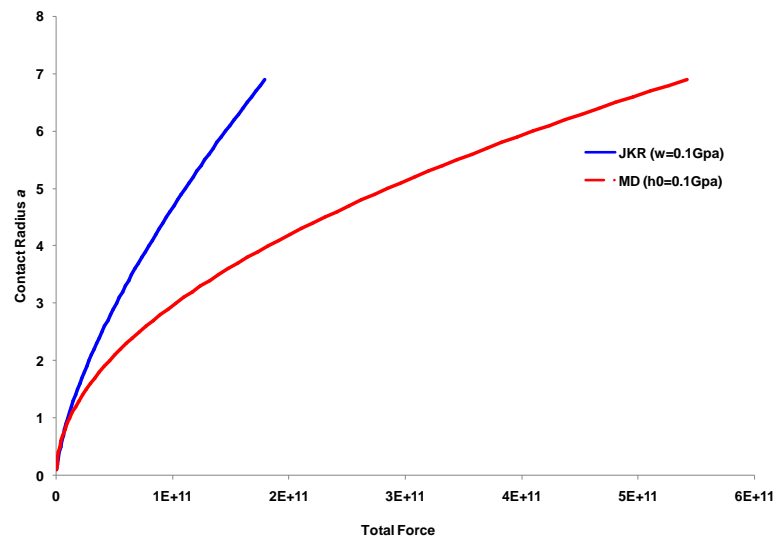
Fig. 2.20 Contact radius versus total force for both the JKR and the MD models (w=h0=0.1 GPa)

Fig. 2.21 Contact radius versus total force for both the JKR and the MD models (w=h0=1 GPa)

Figures 2.22-2.24 study the normal stress changes with the radius r. With r increasing, the negative value of the normal stress decreases. There are no big changes among the three cases discussed and given by a same radius r, the negative value of the normal stress from the JKR adhesive contact model is always larger than those from the MD adhesive contact model.
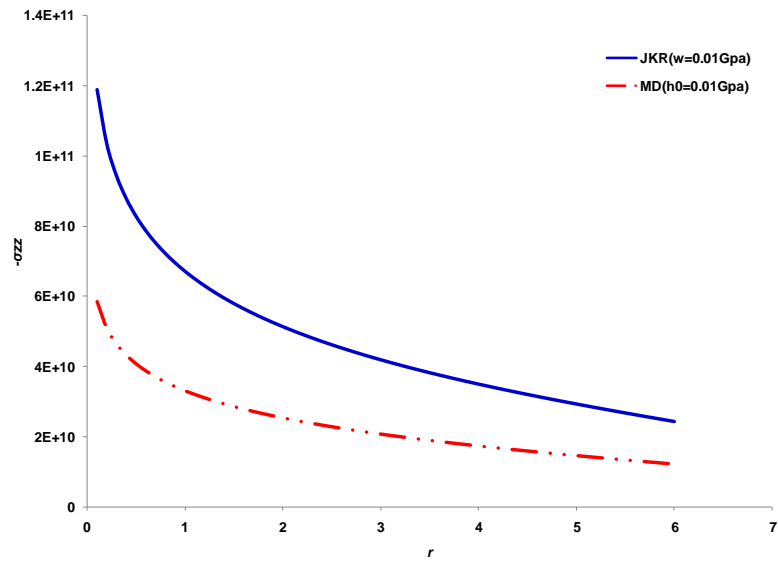
Fig. 2.22 Normal stress versus *r* for both the JKR and the MD models (w=h0=0.01 GPa)

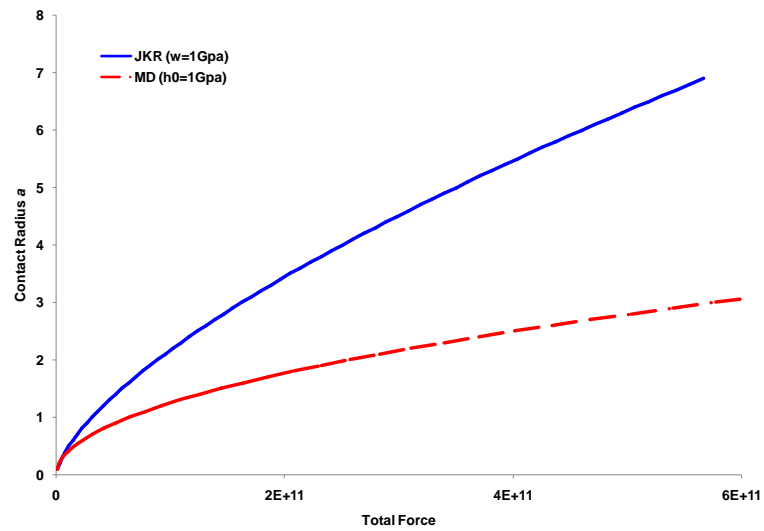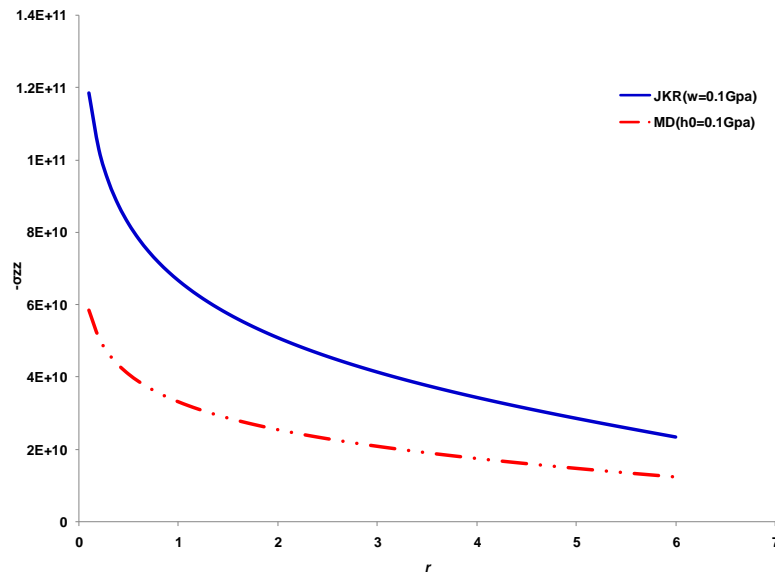**Fig. 2.23 Normal stress versus *r* for both the JKR and the MD models (w=h0=0.1 GPa)**
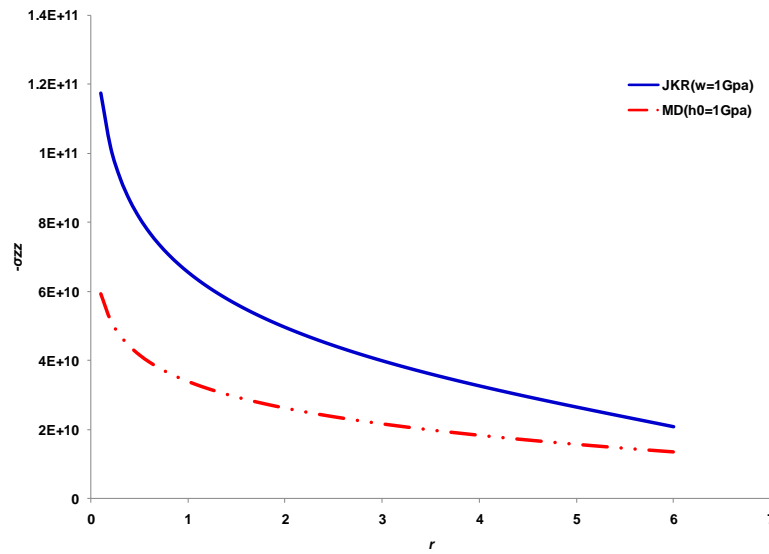
Fig. 2.24 Normal stress versus _r_ for both the JKR and the MD models (w=h0=1 GPa)

If the half-included angle α of the conical frustum punch is set at zero and use the selected isotropic material shown in Table 2.2, then the problem is reduced to solve the adhesive contact problem of a flat-end cylindrical punch with radius a indenting an isotropic elastic half space. To analyze the numerical results for this case, the results in Yang and Li [23] are compared with the ones shown in the following part. Yang and Li study the adhesion of a rigid flat-end cylinder with an incompressible elastic film. In the case of the cylinder radius much larger than the film thickness, the film can be seemed as an elastic half space. Therefore, the JKR adhesive contact model for analyzing the adhesion between the flat-end cylinder and isotropic elastic half space are used and compared with the MD model results.

Figures 2.25-2.27 show the negative normal stress increases with the radius distance increasing. As the constant values increase from 0.01 GPa to 1 GPa, the normal

stress from the JKR model decreases until the normal stress from the MD model is larger than the ones from the JKR model. Especially when $w = h_0 = 1$ GPa, in the region $r < 4$, the results from the JKR and MD adhesive contact models are almost identical. Thus, those constants, different pressure constant h_0 and energy of adhesion w, affect the normal stress significantly.
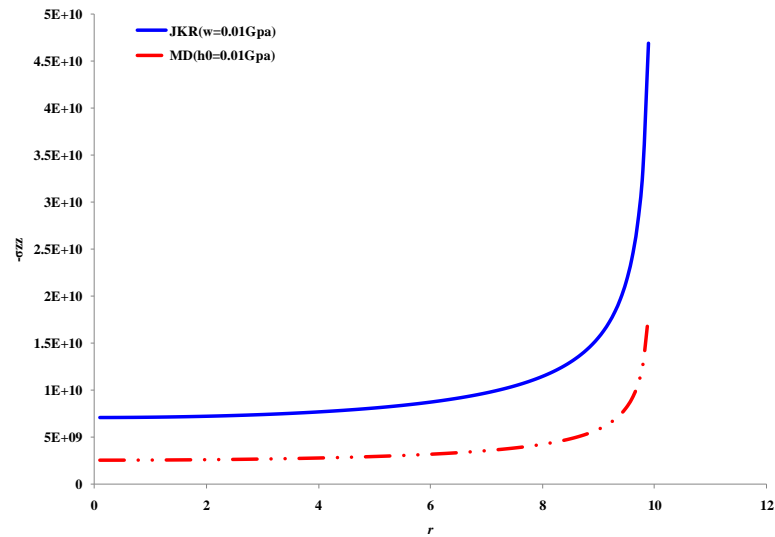
Fig. 2.25 Normal stress versus r for flat-end cylindrical punch (w=h0=0.01 GPa)
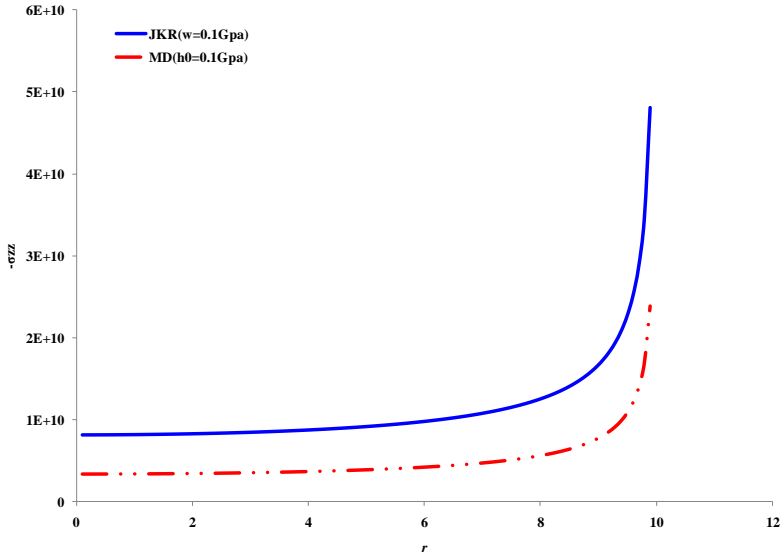
Fig. 2.26 Normal stress versus r for flat-end cylindrical punch (w=h0=0.1 GPa)
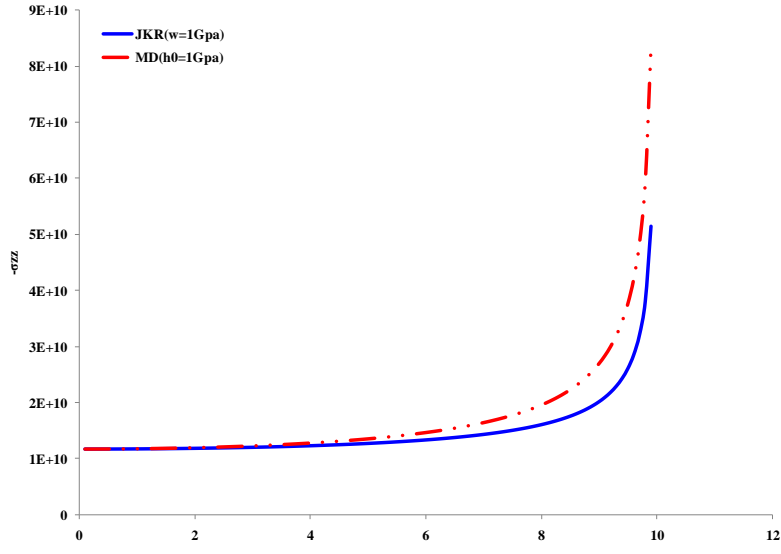
Fig. 2.27 Normal stress versus r for flat-end cylindrical punch (w=h0=1 GPa)

Figures 2.28-2.30 detail the total force versus the penetration depth of the flat-end cylindrical punch. As clearly seen, the total force increases as the penetration depth

increases. As the constant values increase from 0.01 GPa to 1 GPa, the difference between these two models becomes larger and larger until the two models have no cross point. The total force calculated from the JKR adhesive contact model keeps above than those from the MD model.
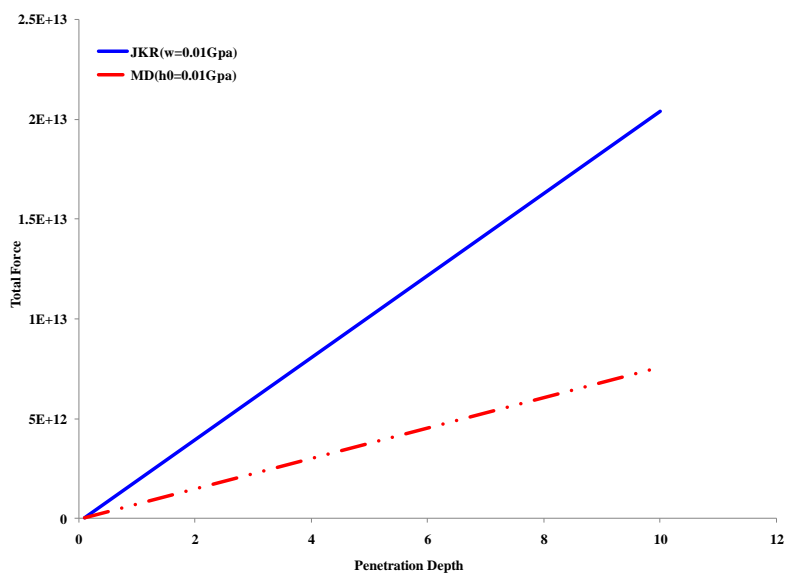
Fig. 2.28 Total force versus penetration depth for flat-end cylindrical punch (w=h0=0.01 GPa)
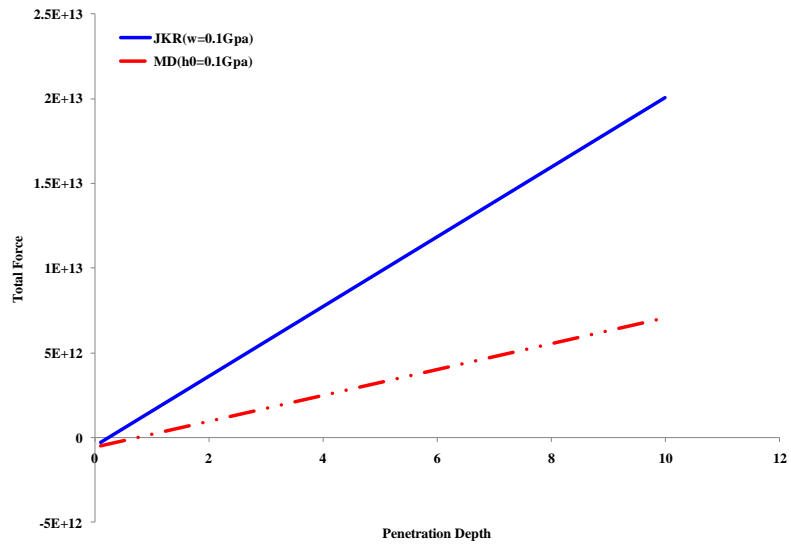
Fig. 2.29 Total force versus penetration depth for flat-end cylindrical punch (w=h0=0.1 GPa)
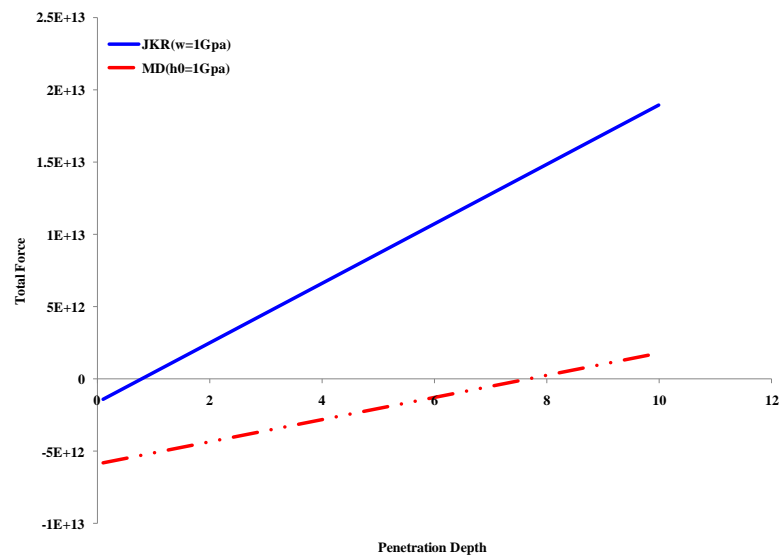
Fig. 2.30 Total force versus penetration depth for flat-end cylindrical punch (w=h0=1 GPa)

2.6. Conclusion

By applying superposition principle, the adhesive contact problem of a conical frustum punch with a transversely isotropic elastic half space can be solved by combing the Hertz contact and Boussinesq contact together. For this chapter, the MD model is used to evaluate the adhesive contact, which considering an external crack near the contact edges with the contact radius changing from a to c. In this zone, the constant pressure distribution h_0 is assumed. The Boussinesq contact is added in order to counteract the singularity of the external crack. Seen from the numerical analysis, the displacement method and stress method do not have significant differences. However, the penetration depth, normal stress, normal displacement and total force would change greatly if h_0 is set various values. The adhesive contact model such as the JKR, DMT and MD models can be extended from isotropic material into transversely isotropic material.

CHAPTER III

ADHESIVE CONTACT OF A CONICAL

FRUSTUM PUNCH WITH AN

ORTHOTROPIC ELASTIC HALF SPACE

3.1. Introduction

Compared with those for transversely isotropic materials, but also very few studies have been conducted for indentation of orthotropic elastic materials.

Willis [24] presented a closed-form solution of the Hertz contact of two anisotropic bodies, which covers both transversely isotropic and orthotropic elastic materials. By using the Fourier transform method, the solution for the problem of a point load applied on an elastic anisotropic half space was derived. Then, by integrating the solution of the point load case over the contact area, the complete expressions for both the displacement and stress components of the Hertz contact were obtained.

Willis [25] later provided a closed-form solution of the Boussinesq contact of a flat-end cylindrical punch on an anisotropic half space. Different pressure distributions in the contact area were discussed.

Swanson [26] studied the spherical indentation into an orthotropic elastic half space by using Willis' method.

Figure 3.1 shows a conical frustum indenting an orthotropic half space. The adhesion is considered. The parameters are shown below.
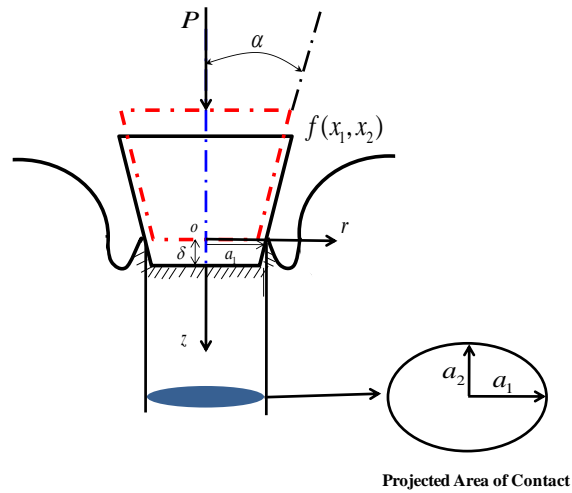
Fig. 3.1 Adhesive contact of a conical frustum punch with an orthotropic elastic half space.

The projected contact area is assumed to be elliptical, and the boundary conditions are prescribed to be the same as those for the transversely isotropic material given in Eqs. (2.1) and (2.2).

3.2. General Solutions for Conical Frustum Indentation into an Orthotropic Half Space

This section will follow the formulation of Willis [24,25] and Swanson [26] to derive an analytical solution for the contact problem shown in Fig.3.1.

Zhang [22] gave a pressure distribution form for the JKR adhesive contact model, which is separated into two parts. One part is the Hertz pressure and the other is the Boussinesq pressure. For the current problem with a conical frustum punch, modifications are necessary due to the flat-end contact surface. For $0 \le r < a_b$ (flat-end),

the Hertz pressure is taken to be $p_0(1-\dfrac{x_1^2}{a_1^2}-\dfrac{x_2^2}{a_2^2})^{-1/2}$, which is the same as the pressure

distribution for the Boussinesq contact assumed by Willis [25]. The reason for this is

that, in this region the prescribed normal displacement u_z equals to the punch

penetration depth δ, which is a zero order polynomial of x_1 and x_2. For $a_b \leq r < a$, the

Hertz pressure is assumed to have the form of $p_0 \cosh^{-1}[(\dfrac{x_1^2}{a_1^2}+\dfrac{x_2^2}{a_2^2})^{-1/2}]$, as was

mentioned in Vlassak et al.[27]. However, for both the regions $0 \leq r < a_b$ and $a_b \leq r < a$,

the pressure distribution for the Boussinesq contact is $p_0'(1-\dfrac{x_1^2}{a_1^2}-\dfrac{x_2^2}{a_2^2})^{-1/2}$. Then, the

pressure distribution for the adhesive contact of the conical frustum indenter can be

obtained easily by adding the Hertz pressure and the Boussinesq pressure.

3.2.1 Displacement Formulation Due to a Unit Point Load

In a Cartesian coordinate system for an orthotropic elastic materials, the stress-

strain relations are given by

$$\begin{aligned}
\sigma_{11} &= c_{11}\varepsilon_{11} + c_{12}\varepsilon_{22} + c_{13}\varepsilon_{33}, \\
\sigma_{22} &= c_{12}\varepsilon_{11} + c_{22}\varepsilon_{22} + c_{23}\varepsilon_{33}, \\
\sigma_{33} &= c_{13}\varepsilon_{11} + c_{23}\varepsilon_{22} + c_{33}\varepsilon_{33}, \\
\sigma_{23} &= 2c_{44}\varepsilon_{23}, \\
\sigma_{31} &= 2c_{55}\varepsilon_{31}, \\
\sigma_{12} &= 2c_{66}\varepsilon_{12},
\end{aligned} \tag{3.1}$$

And the strain-displacement relations are

$$\varepsilon_{11} = \frac{\partial v_1}{\partial x_1}, \qquad \varepsilon_{22} = \frac{\partial v_2}{\partial x_2}, \qquad \varepsilon_{33} = \frac{\partial v_3}{\partial x_3},$$

$$\varepsilon_{12} = \frac{1}{2}(\frac{\partial v_1}{\partial x_2} + \frac{\partial v_2}{\partial x_1}),$$

$$\varepsilon_{23} = \frac{1}{2}(\frac{\partial v_2}{\partial x_3} + \frac{\partial v_3}{\partial x_2}),$$

$$\varepsilon_{31} = \frac{1}{2}(\frac{\partial v_3}{\partial x_1} + \frac{\partial v_1}{\partial x_3}),$$

(3.2)

where v_1, v_2 and v_3 are the three displacement components in the absence of body forces

$$\frac{\partial \sigma_{11}}{\partial x_1} + \frac{\partial \sigma_{12}}{\partial x_2} + \frac{\partial \sigma_{13}}{\partial x_3} = 0,$$

$$\frac{\partial \sigma_{12}}{\partial x_1} + \frac{\partial \sigma_{22}}{\partial x_2} + \frac{\partial \sigma_{23}}{\partial x_3} = 0,$$

$$\frac{\partial \sigma_{13}}{\partial x_1} + \frac{\partial \sigma_{23}}{\partial x_2} + \frac{\partial \sigma_{33}}{\partial x_3} = 0.$$

(3.3)

using Eqs. (3.1) and (3.2) in Eq. (3.3) gives

$$c_{11}v_{1,11} + c_{66}v_{1,22} + c_{55}v_{1,33} + (c_{12} + c_{66})v_{2,12} + (c_{13} + c_{55})v_{3,13} = 0,$$

$$c_{22}v_{2,22} + c_{66}v_{2,11} + c_{44}v_{2,33} + (c_{12} + c_{66})v_{1,12} + (c_{23} + c_{44})v_{3,23} = 0, \quad (3.4a,b,c)$$

$$c_{33}v_{3,33} + c_{55}v_{3,11} + c_{44}v_{3,22} + (c_{13} + c_{55})v_{1,13} + (c_{23} + c_{44})v_{2,23} = 0,$$

The Fourier transforms in the x_1- and x_2-directions are defined by

$$\tilde{f}(\xi_1) = \frac{1}{\sqrt{2\pi}} \int_{-\infty}^{\infty} f(x_1) \exp(i\xi_1 x_1) dx_1$$

(3.5)

$$\tilde{f}(\xi_2) = \frac{1}{\sqrt{2\pi}} \int_{-\infty}^{\infty} f(x_2) \exp(i\xi_2 x_2) dx_2$$

Taking the Fourier transforms on Eqs.(3.4a,b,c) then yields

$$(c_{11}\xi_1^2 + c_{66}\xi_2^2)\tilde{v}_1 - c_{55}\tilde{v}_{1,33} + \xi_1\xi_2(c_{12} + c_{66})\tilde{v}_2 + i\xi_1(c_{13} + c_{55})\tilde{v}_{3,3} = 0,$$

$$\xi_1\xi_2(c_{12} + c_{66})\tilde{v}_1 + (c_{66}\xi_1^2 + c_{22}\xi_2^2)\tilde{v}_2 - c_{44}\tilde{v}_{2,33} + i\xi_2(c_{23} + c_{44})\tilde{v}_{3,3} = 0, \quad (3.6)$$

$$i\xi_1(c_{13} + c_{55})\tilde{v}_{1,3} + i\xi_2(c_{23} + c_{44})\tilde{v}_{2,3} + (c_{55}\xi_1^2 + c_{44}\xi_2^2)\tilde{v}_3 - c_{33}\tilde{v}_{3,33} = 0,$$

Consider the solution of the form,

$$\begin{Bmatrix} \tilde{v}_1 \\ \tilde{v}_2 \\ \tilde{v}_3 \end{Bmatrix} = \begin{Bmatrix} A_1 \\ A_2 \\ A_3 \end{Bmatrix} \exp(i\varepsilon x_3) \tag{3.7}$$

using Eq.(3.7)in Eq. (3.6) leads to

$$\begin{pmatrix} c_{11}\xi_1^2 + c_{66}\xi_2^2 + c_{55}\varepsilon^2 & \xi_1\xi_2(c_{12}+c_{66}) & -\varepsilon\xi_1(c_{13}+c_{55}) \\ & c_{66}\xi_1^2 + c_{22}\xi_2^2 + c_{44}\varepsilon^2 & -\varepsilon\xi_2(c_{23}+c_{44}) \\ sym. & & c_{55}\xi_1^2 + c_{44}\xi_2^2 + c_{33}\varepsilon^2 \end{pmatrix} \begin{Bmatrix} A_1 \\ A_2 \\ A_3 \end{Bmatrix} = \begin{Bmatrix} 0 \\ 0 \\ 0 \end{Bmatrix} \tag{3.8}$$

In order to get a non trivial solution, the determinant of the coefficient matrix has to vanish. That is,

$$\begin{vmatrix} \dfrac{c_{11}}{c_{55}}\xi_1^2 + \dfrac{c_{66}}{c_{55}}\xi_2^2 + \varepsilon^2 & \xi_1\xi_2\dfrac{(c_{12}+c_{66})}{c_{55}} & -\varepsilon\xi_1\dfrac{(c_{13}+c_{55})}{c_{55}} \\ & \dfrac{c_{66}}{c_{44}}\xi_1^2 + \dfrac{c_{22}}{c_{44}}\xi_2^2 + \varepsilon^2 & -\varepsilon\xi_2\dfrac{(c_{23}+c_{44})}{c_{44}} \\ sym. & & \dfrac{c_{55}}{c_{33}}\xi_1^2 + \dfrac{c_{44}}{c_{33}}\xi_2^2 + \varepsilon^2 \end{vmatrix} = 0, \tag{3.9}$$

Define,

$$b_1 = \frac{c_{11}}{c_{55}},\ b_2 = \frac{c_{66}}{c_{55}},\quad b_3 = \frac{c_{66}}{c_{44}},\quad b_4 = \frac{c_{22}}{c_{44}},\quad b_5 = \frac{c_{55}}{c_{33}},$$

$$b_6 = \frac{c_{44}}{c_{33}},\quad b_7 = \frac{c_{12}+c_{66}}{c_{55}},\quad b_8 = \frac{c_{13}+c_{55}}{c_{55}},\quad b_9 = \frac{c_{23}+c_{44}}{c_{44}}. \tag{3.10}$$

inserting Eq.(3.10) into Eq.(3.9) computing the determinant will result in

$$\varepsilon^6 + (e_1\xi_1^2 + e_2\xi_2^2)\varepsilon^4 + (e_3\xi_1^4 + e_4\xi_1^2\xi_2^2 + e_5\xi_2^4)\varepsilon^2 + (e_6\xi_1^6 + e_7\xi_1^4\xi_2^2 + e_8\xi_1^2\xi_2^4 + e_9\xi_2^6) = 0 \tag{3.11}$$

where

$$e_1 = b_1 + b_3 + b_5 - b_8^2, \quad e_2 = b_2 + b_4 + b_6 - b_9^2,$$

$$e_3 = b_1 b_3 + b_1 b_5 + b_3 b_5 - b_3 b_8^2,$$

$$e_4 = b_2 b_3 + b_1 b_4 + b_2 b_5 + b_4 b_5 + b_1 b_6 + b_3 b_6 + 2 b_7 b_8 b_9 - (b_4 b_8^2 + b_1 b_9^2 + b_7^2)$$

$$e_5 = b_2 b_4 + b_2 b_6 + b_4 b_6 - b_2 b_9^2, \quad e_6 = b_1 b_3 b_5, \quad e_7 = b_2 b_3 b_5 + b_1 b_4 b_5 + b_1 b_3 b_6 - b_5 b_7^2$$

$$e_8 = b_2 b_4 b_5 + b_2 b_3 b_6 + b_1 b_4 b_6 - b_5 b_7^2, \quad e_9 = b_2 b_4 b_6$$

$$\tag{3.12}$$

The six roots of Eq.(3.11) have the form:

$$\varepsilon_{1,2} = \pm \beta_1, \qquad \varepsilon_{3,4} = \pm \beta_2, \qquad \varepsilon_{5,6} = \pm \beta_3, \tag{3.13}$$

For each root $\varepsilon_i (i = 1, 2...6)$, substituting it into Eq.(3.8) and solving the equation system with two independent equations will lead to two unknowns $(A_1 / A_3)_i$ and $(A_2 / A_3)_i$. The solution of Eq.(3.6) can then expressed as

$$\begin{Bmatrix} \tilde{v}_1 \\ \tilde{v}_2 \\ \tilde{v}_3 \end{Bmatrix} = \sum_{k=1}^{6} \begin{Bmatrix} (A_1 / A_3)_k \\ (A_2 / A_3)_k \\ 1 \end{Bmatrix} (A_3)_k \exp(i\varepsilon_k x_3), \tag{3.14}$$

where $(A_3)_k$ $(k = 1, 2...6)$ are six unknown constants. Three of these six constants associated with the three roots whose imaginary parts are negative will be taken to be zero to satisfy the boundary conditions of the displacements vanishing at $x_3 \to \infty$. The remain three constants (say, $(A_3)_1$, $(A_3)_2$ and $(A_3)_3$) will be determined from the following boundary conditions.

$$\sigma_{13}(x_1, x_2, 0) = 0, \quad \sigma_{23}(x_1, x_2, 0) = 0, \quad \sigma_{33}(x_1, x_2, 0) = -\delta(x_1)\delta(x_2) \tag{3.15a}$$

using Eqs.(3.1) and (3.2) in Eq.(3.15a) gives

$$\begin{cases} c_{55}(v_{3,1}+v_{1,3})|_{x_3=0}=0 \\ c_{44}(v_{2,3}+v_{3,2})|_{x_3=0}=0 \\ c_{13}v_{1,1}|_{x_3=0}+c_{23}v_{2,2}|_{x_3=0}+c_{33}v_{3,3}|_{x_3=0}=-\delta(x_1)\delta(x_2) \end{cases}$$ (3.15b)

Taking the Fourier transforms on each of Eq.(3.15b) and then using Eq.(3.14) will yield

$$\begin{cases} \xi_1\tilde{v}_3|_{x_3=0}+i\tilde{v}_{1,3}|_{x_3=0}=0 \\ i\tilde{v}_{2,3}|_{x_3=0}+\xi_2\tilde{v}_3|_{x_3=0}=0 \\ \xi_1 c_{13}\tilde{v}_1|_{x_3=0}+\xi_2 c_{23}\tilde{v}_2|_{x_3=0}+ic_{33}\tilde{v}_{3,3}|_{x_3=0}=-\frac{1}{2\pi} \end{cases}$$ (3.15c)

The displacement components v_i $(i=1,2,3)$ can then be obtained through inverse Fourier transforms to be

$$\sum_{i=1}^{3}[\varepsilon_i(A_1/A_3)_i-\xi_1](A_3)_i=0,$$

$$\sum_{i=1}^{3}[\varepsilon_i(A_2/A_3)_i-\xi_2](A_3)_i=0,$$ (3.16)

$$\sum_{i=0}^{3}[c_{13}\xi_1(A_1/A_3)_i+c_{23}\xi_2(A_2/A_3)_i-c_{33}\varepsilon_i](A_3)_i=\frac{-1}{2\pi}.$$

Solving Eq.(3.16) will lead to the determination of $(A_3)_i$ $(i=1,2,3)$, thereby the completing solution given in Eqs.(3.7) and (3.13) in transformed domain.

$$v_1=\frac{1}{2\pi}\int\int_{-\infty}^{\infty}\tilde{v}_1 e^{-i(\xi_1 x_1+\xi_2 x_2)}d\xi_1 d\xi_2,$$

$$v_2=\frac{1}{2\pi}\int\int_{-\infty}^{\infty}\tilde{v}_2 e^{-i(\xi_1 x_1+\xi_2 x_2)}d\xi_1 d\xi_2,$$ (3.17a,b,c)

$$v_3=\frac{1}{2\pi}\int\int_{-\infty}^{\infty}\tilde{v}_3 e^{-i(\xi_1 x_1+\xi_2 x_2)}d\xi_1 d\xi_2,$$

where $\tilde{v}_1$ - $\tilde{v}_3$ are given in Eqs.(3.14) and (3.16).

3.2.2 The Adhesive Contact by Using the JKR Model

The contact pressure is taken to have the following form ([22] and [27]),

$$p(x_1, x_2) = \begin{cases} (p_0 - p_0')(1 - \dfrac{x_1^2}{a_1^2} - \dfrac{x_2^2}{a_2^2})^{-1/2}, & 0 \le r < a_b \\[4mm] p_0 \cosh^{-1}[\dfrac{1}{(x_1^2/a_1^2 + x_2^2/a_2^2)^{1/2}}] - p_0'(1 - \dfrac{x_1^2}{a_1^2} - \dfrac{x_2^2}{a_2^2})^{-1/2}, & a_b \le r < a \end{cases}$$

(3.18a,b)

The surface displacements due to this contact pressure can then be obtained by integrating the displacements induced by the unit point load over the contact area. That is, in the contact area $0 \le r \le a_b$, the vertical surface displacement is given by

$$u^{in}{}_3(x_1, x_2, 0) = \iint_S (p_0 - p_0')(1 - \frac{x_1'^2}{a_1} - \frac{x_2'^2}{a_2})^{-1/2} w(x_1 - x_1', x_2 - x_2')dx_1'dx_2'$$

$$= \iint_S (p_0 - p_0')(1 - \frac{x_1'^2}{a_1} - \frac{x_2'^2}{a_2})^{-1/2}$$

$$\frac{1}{2\pi}\iint \tilde{w}(\xi_1, \xi_2)\exp(-i\xi_1(x_1 - x_1') - i\xi_2(x_2 - x_2'))d\xi_1 d\xi_2 dx_1'dx_2'$$

(3.19)

where

$$w(x_1, x_2) = v_3(x_1, x_2, 0)$$

(3.20)

is the vertical surface displacement due to the point load obtained in Section 3.2.2, and use has been made of Eq.(3.17c) and (3.18a).

Eq.(3.19) can be evaluated to give (Willis[25] and Swanson[26])

$$u^{in}{}_3(x_1, x_2, 0) = \frac{\pi}{2}(p_0 - p_0')\oint \tilde{w}(\eta_1/a_1, \eta_2/a_2)ds$$

$$= \frac{\pi}{2}(p_0 - p_0')a_2\int_0^{2\pi} \tilde{w}(\chi\eta_1, \eta_2)d\theta$$

(3.21)

where,

$$\chi = \frac{a_2}{a_1}, \quad \eta_1 = \cos(\theta), \quad \eta_2 = \sin(\theta)$$

(3.22)

The depth of penetration is then obtained from Eq.(3.21) to be

$$\delta = u^{in}_{\ 3}(0,0,0) = \frac{\pi}{2}(p_0 - p'_0)a_2 \int_0^{2\pi} \tilde{w}(\chi\eta_1, \eta_2)d\theta$$

(3.23)

Similarly in the contact area $a_b < r \le a$, the vertical surface displacement is

$$u^{out}_{\ 3}(x_1,x_2,0) = \iint_S [p_0 \cosh^{-1}[\frac{1}{(x_1'^2/a_1^2 + x_2'^2/a_2^2)^{1/2}}] - p'_0(1 - \frac{x_1'^2}{a_1^2} - \frac{x_2'^2}{a_2^2})^{-1/2}]$$
$$w(x_1 - x_1', x_2 - x_2', 0)dx_1'dx_2'$$

(3.24)

$$u^{out}_{\ 3}(x_1,x_2,0) = \frac{p_0 i}{2\pi} \oint \tilde{w}(\eta_1/a_1, \eta_2/a_2)ds \iint_{y'_\lambda < 1} \frac{\cosh^{-1}(1/(y_1'^2 + y_2'^2)^{1/2})}{mx_3 - \eta_1 y_1 - \eta_2 y_2 + \eta_1 y_1' + \eta_2 y_2'}dy_1'dy_2'$$
$$- p'_0 a_2 \int_0^{2\pi} \tilde{w}(\chi\eta_1, \eta_2)d\theta,$$

(3.25)

where

$$y_1 = \frac{x_1}{a_1}, \qquad y_2 = \frac{x_2}{a_2}$$
$$y_1' = \frac{x_1'}{a_1}, \qquad y_2' = \frac{x_2'}{a_2}$$

(3.26)

To evaluate the integral, use will be made of the following expression [28]

$$\cosh^{-1}(1/z) = \ln(2/z) - \sum_{n=1}^{\infty} \frac{(2n)!}{2^{2n}(n!)^2 2n} z^{2n}$$

(3.27)

3.2.3 The Numerical Results for the General Orthotropic Solutions

Due to the complex integration in eqn (3.26), use the approximation integration method in Maple to get the numerical results. The solutions discussed in Section 3.2.2 could be used for any anisotropic material. Therefore, for convenience, the transversely isotropic material is selected and the contact area is assumed as a circle shape. The

comparisons are made between the reduced solutions of transversely isotropic material from Section 3.2.2 and the closed-form solutions shown in Chapter II.

The following results show the normalized pressure distribution, displacement and normal stress.

The normalized pressure distribution,

$$\hat{p}(r) = \begin{cases} (1-\rho)(1-\gamma^2)^{-1/2}, & 0 \le r < a_b \\ \cosh^{-1}(1/\gamma) - \rho(1-\gamma^2)^{-1/2}, & a_b \le r < a \end{cases} \tag{3.28}$$

with,

$$\hat{p}(r) = \frac{p(r)}{p_0},$$

$$\rho = \frac{p_0'}{p_0},$$

$$\gamma = \frac{r}{a}$$

Figures 3.2-3.3 show the assumed pressure distribution for the JKR adhesive contact model for the flat-end region ($0 \le r < a_b$) and the conical region ($a_b \le r < a$), respectively. As ρ varies from 0.1 to 1.5, the pulling force added on the punch becomes larger than the indenting force. For the flat-end region of the punch, the normalized pressure distribution decreases to zero and turns out to increase in the opposite direction when ρ increases. For the conical region, the pressure distribution decreases when ρ increases. When γ equals exactly to one, the pressure distribution goes to infinity.
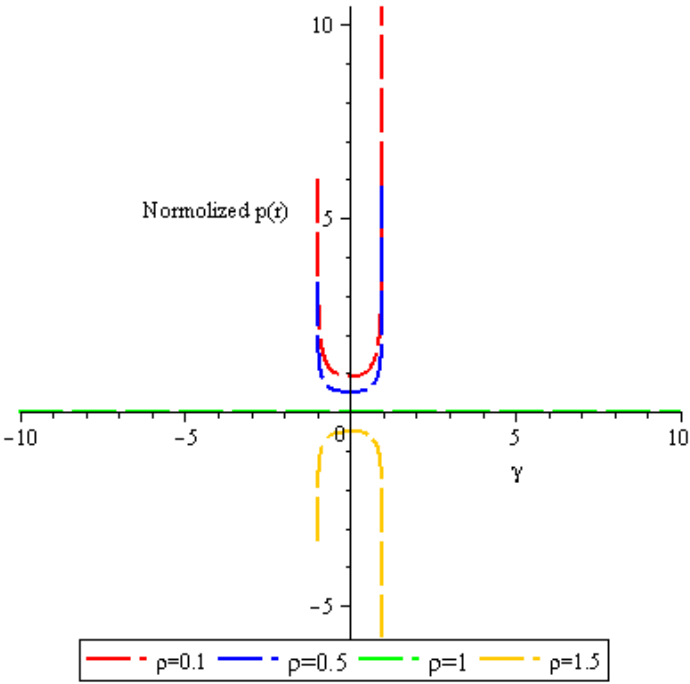
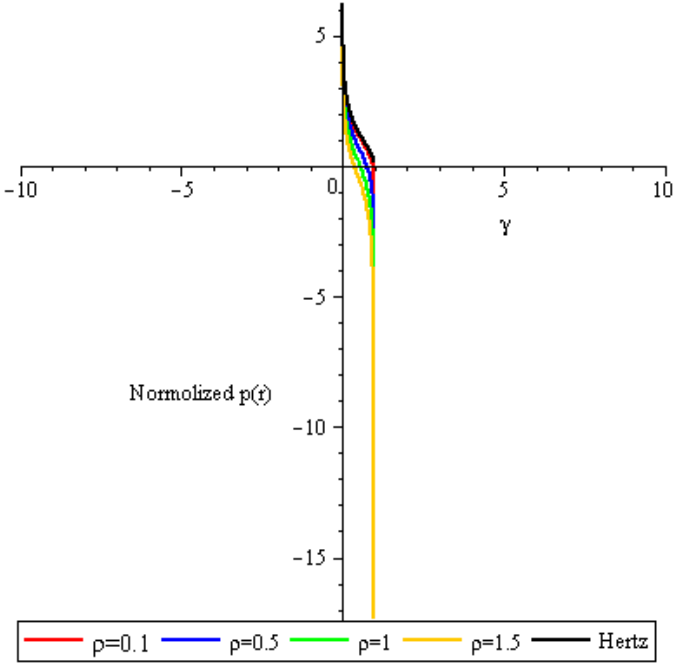**Fig.3.2 Pressure distribution when** $0 \le r < a_b$

Fig.3.3 Pressure distribution when $a_b \le r < a$

Figures 3.4 – 3.7 indicate that the comparisons for the penetration depth of the conical frustum punch changes with the contact radius among displacement method, stress method and approximation method. For $p_0' = 0.1Gpa$, p_0 increases from 0.7 GPa to 10 GPa. Seen from Fig. 3.4, the results of the displacement method, stress method and the approximation method when p_0 equals to 7 GPa have no large difference and almost overlap to a single line. However, in the cases when p_0 equals to 0.1 GPa, 5 GPa or 10 GPa, the results show a huge discrepancy compared with the displacement and stress methods. This means when the pulling out force is fixed in the first place, p_0 can affect the penetration depth of the conical frustum punch significantly, which can also be illustrated from Fig. 3.5 to Fig. 3.7. As p_0' increases from 0.1 GPa to 1.5 GPa, the interval between the displacement and stress methods increases.

Fig. 3.4 Penetration depth versus contact radius comparisons between displacement method, stress method and approximation ($p'_0 = 0.1Gpa$)

Fig. 3.5 Penetration depth versus contact radius comparisons between displacement method, stress method and approximation ($p'_0 = 0.5Gpa$)

Fig. 3.6 Penetration depth versus contact radius comparisons between displacement method, stress method and approximation ($p'_0 = 1 Gpa$)

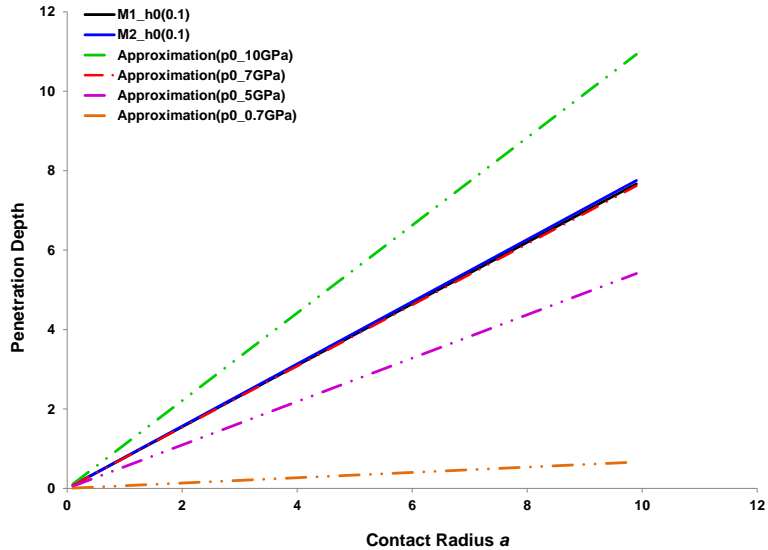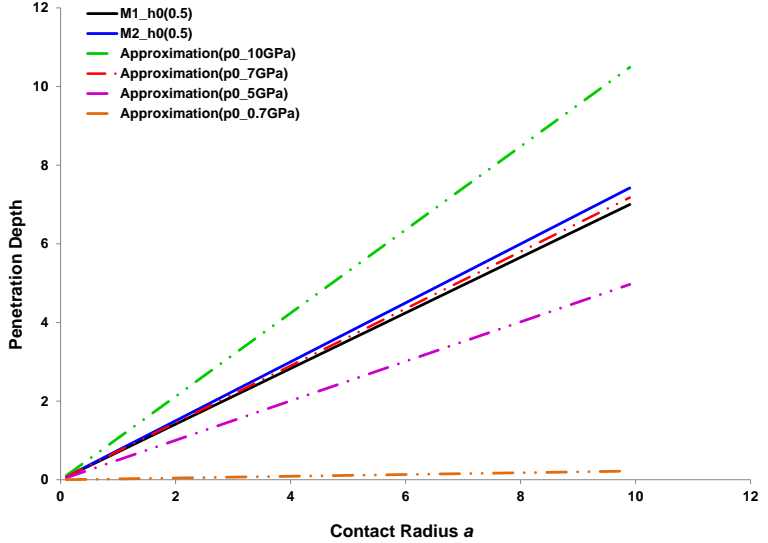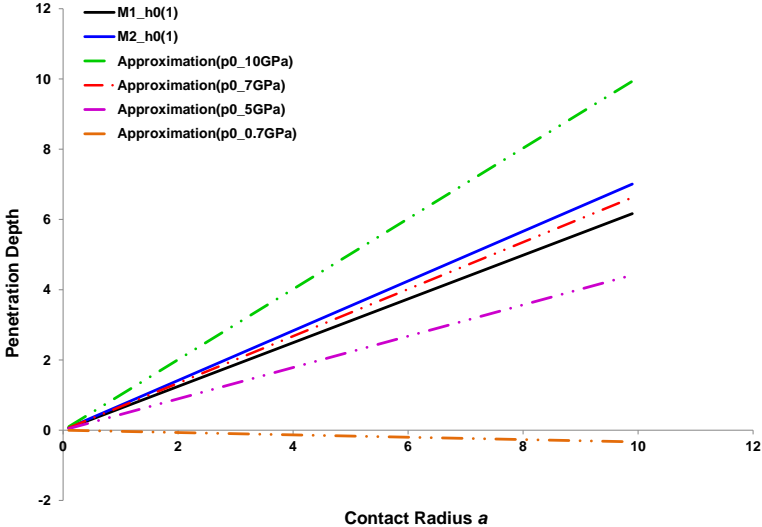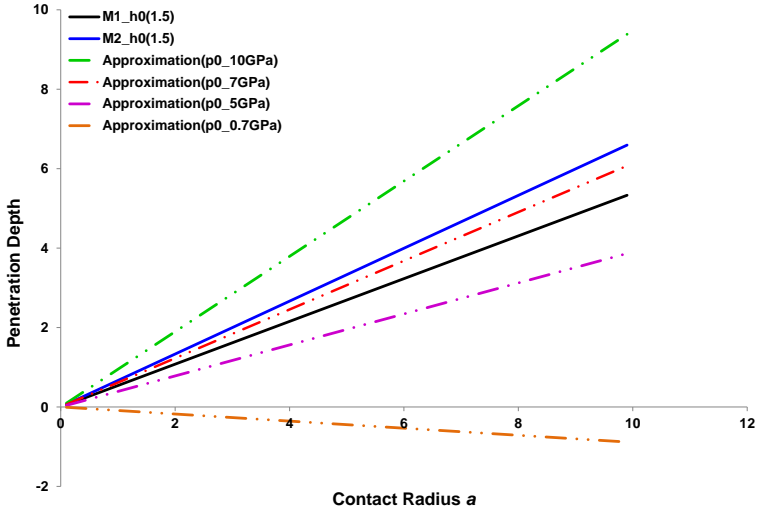**Fig. 3.7 Penetration depth versus contact radius comparisons between displacement method, stress method and approximation ($p'_0 = 1.5 Gpa$)**

Figures 3.8 – 3.10 detail the normal displacement changes with the contact radius

when p_0 and α increase for displacement, stress and approximation methods. p_0' is

fixed at 0.1 GPa, 0.5 GPa and 1 GPa, respectively. As seen from these three plots, the

normal displacement decreases as the contact radius increases. Both of displacement and

stress methods appear the linear relationship between the normal displacement and

contact radius. As the half-included angle α varies from 30 degrees to 60 degrees with

the interval of 15 degrees, the slope of the line becomes larger and especially when p_0'

equals to 0.1 GPa, these two methods have no big difference. As p_0' increases, the

difference between these two methods becomes larger and the intersection point of three

lines becomes away from the x axis. For the approximation method, it is easily

illustrated that both p_0 and α can influence the normal displacement compared with the

numerical results from displacement and stress methods. With p_0 increases from

$2 \cdot 10^{13}$ Pa to 10^{14}, the intersection point of the approximation and the exact solutions

becomes smaller and these three methods start and end at the same points for each case.

Fig. 3.8 Normal displacement for conical part versus contact radius comparisons between displacement method, stress method and approximation ($p'_0 = 0.1 Gpa$)
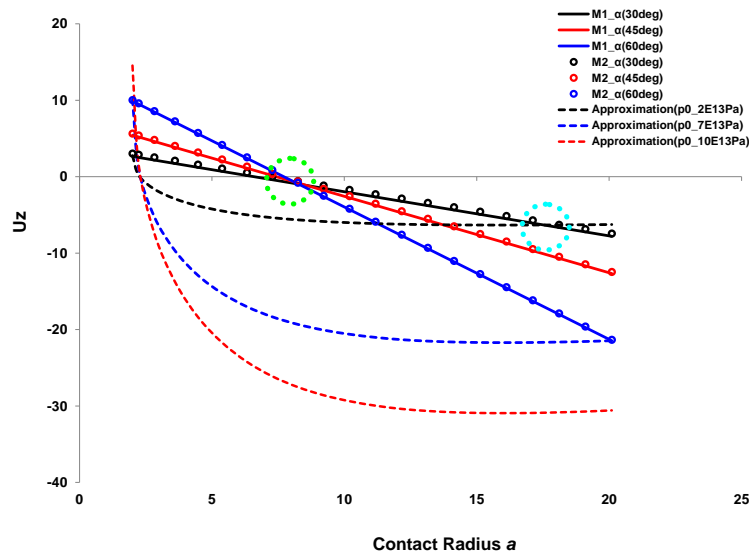
Fig. 3.9 Normal displacement for conical part versus contact radius comparisons between displacement method, stress method and approximation ($p'_0 = 0.5 Gpa$)
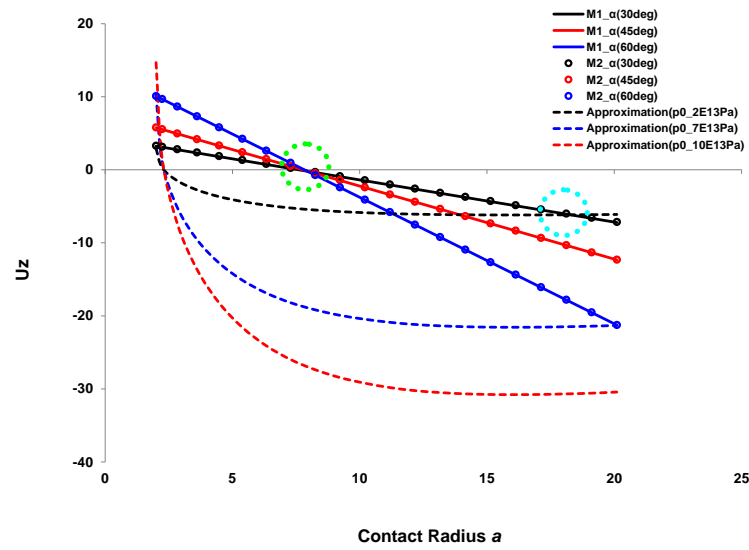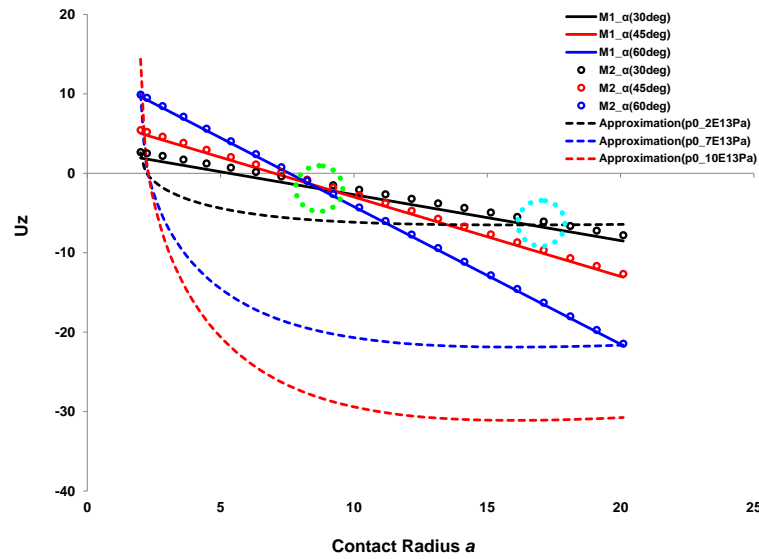
Fig. 3.10 Normal displacement for conical part versus contact radius comparisons between displacement method, stress method and approximation ($p_0' = 1Gpa$)

3.3. Conclusion

This chapter studies the approximation method of the conical frustum punch indenting the general orthotropic half space and the closed-form solutions for the special orthotropic half space. For the general orthotropic material, the pressure distribution for the contact area is assumed as the ellipsoidal shape and the Fourier transform is used.

CHAPTER IV

CONCLUSION

The adhesive contact problems of a conical frustum punch with a transversely isotropic or an orthotropic elastic half space are analytically achieved. To solve a conical frustum punch indenting a transversely isotropic elastic half space, the adhesive contact is formed of the Hertz contact and the Boussinesq contact based on the superposition principle. By using the harmonic potential function method and Hankel transform, a closed-form solution of the displacement and stress is obtained. The MD adhesive contact model solved by the former work for isotropic material is extended to solve the transversely isotropic material. Inside the cohesive contact region, the external crack and constant pressure distribution are assumed. The constant h_0 can affect the normal displacement, normal stress and total force of the conical frustum punch.

To analyze the adhesive contact problems of a conical frustum punch with an orthotropic half space, the Fourier transform is used to solve the problem of a point load applied on the elastic half space. The projected contact area is assumed to be semi-ellipsoidal and the pressure distribution of the JKR adhesive contact model is applied. The approximation method has certain discrepancy compared with the derived closed-form solution of the transversely isotropic material. Along with the pressure distribution constants p_0 and p_0', the half-included angle of the conical frustum punch can influence the normal displacement, normal stress and total force. For the adhesive contact problems of general orthotropic elastic half space, the JKR adhesive contact model can

be extended into an orthotropic material. Finally, the pressure distribution assumption of the project area shape for the general orthotropic materials can affect the numerical results significantly.

For future work, firstly, the Fourier transform method of solving the contact problem of the general orthotropic materials needs to be improved to obtain the exact solutions other than the approximation solutions. Secondly, the pressure distribution of the JKR model needs to be improved for a conical punch profile. Last but not least, do the research on the MD adhesive contact model to check whether it can be extended to solve the contact problem of the general orthotropic materials.

REFERENCES

[1] Hertz, H., 1882, On the Contact of Elastic Solids, *J. Reine Angew. Math.* 92, 156-171.

[2] Bradley, R.S., 1932, The Cohesive Force Between Solid Surface and the Surface Energy of Solids, *phil, Mag.* 13, 853-862.

[3] Johnson, K.L., Kendall, K. and Roberts, A.D., 1971, Surface Energy and the Contact of Elastic Solids, *Proc.R.Soc.Lond.*A 324, 301-313.

[4] Derjaguin, B.V., Muller, V.M. and Toporov, Yu. P., 1975, Effect of Contact Deformation on the Adhesion, *J.Colloid Interface Sci.* 53, 314.

[5] Muller, V.M., Yushenko, V.S. and Derjaguin, B.V., 1980, On the Influence of Molecular Forces on the Deformation of an Elastic Sphere, *J.Colloid Interface Sci.* 77, 91.

[6] Maugis, D., 1992, Adhesion of Spheres: the JKR-DMT Transition Using a Dugdale Model, *J.Colloid Interface Sci.*150, 243-269.

[7] Zhou, S.-S., Gao, X.-L. and He, Q.-C., 2010, A Unified Treatment of Axisymmetric Adhesive Contact Problems Using the Harmonic Potential Function Method, manuscript submitted for publication.

[8] Ejike, U.B.C.O., 1981, The Stress on an Elastic Half-Space Due to Sectionally Smooth-Ended Punch, *J. Elasticity*, 11(4), 395-402

[9] Elliott, H.A., 1948, Three-Dimensional Stress Distributions in Hexagonal Aeolotropic Crystals, *Proc. Cambridge Phil. Soc.* 44, 522-533.

[10] Elliott, H.A., 1949, Axial Symmetric Stress Distributions in Aeolotropic Hexagonal Crystals. The Problem of the Plane and Related Problems, *Proc. Cambridge Phil. Soc.* 45, 621-630.

[11] Hanson, M.T, 1992, The Elastic Field for Conical Indentation Including Sliding Friction for Transverse Isotropy, *J.Appl.Mech.*, 59, S123-S130.

[12] Chen, S., Yan, C., Soh, A., 2008, Non-Slipping JKR Model for Transversely Isotropic Materials, *Int. J. Solids Struct.* 45, 676-687.

[13] Espinasse, L., Keer, L., Borodich, F., Yu, H., Wang, J., 2010, A Note on JKR and DMT Theories of Contact on a Transversely Isotropic Half-Space, *Mech.Mater.*, 42, 477-480.

[14] W. Michael Lai, David Rubin, Erhard Krempl, *Introduction to Continuum Mechanics*.

[15] Titchmarsh, E.C., *Theory of Fourier Integrals* (Oxford, 1937).

[16] Ding H.J., Chen, W.Q., Zhang, L., *Elasticity of Transversely Isotropic Materials* (2006).

[17] Chen, Z.R., Yu, S.W., 2005, Micro-Scale Adhesive Contact of a Spherical Rigid Punch on a Piezoelectric Half-Space, *Compost.Sci.Technol.*, 65, 1372-1381.

[18] Lowemgrub, M., Sneddon I.N., 1965, The Distribution of Stress in the Vicinity of an External Crack in an Infinite Elastic Solids, *Int.J.Eng.Sci.,* 3, 451-460.

[19] Danyluik, H.T., Singh, B.M., Vrbik, J., 1991, Ductile Penny-Shape Crack in a Transversely Isotropic Cylinder, *Int.J.Fracture*, 51, 331-342.

[20] Maugis, D., Barguins, M., 1981, Adhesive Contact of a Conical Punch on an Elastic Half-Space, *J.Physique Lett.*, 42, L-95-L-97.

[21] Sadd, M.H., *Elasticity Theory, Applications, and Numerics* (2005).

[22] Zhang, Y., 2008, Transitions Between Different Contact Models, *J.Adhes.Sci.Technol.*, 22, 699-715.

[23] Yang, F., Li, J.C.M., 2001, Adhesion of a Rigid Punch to an Incompressible Elastic Film, *Langmuir*, 17, 6524-6529.

[24] Willis, J.R., 1966, Hertzian Contact of Anisotropic Bodies, *J.Mech.Phys.Solids.* 14, 163-176.

[25] Willis, J.R., 1967, Boussinesq Problems for an Anisotropic Half-Space, *J.Mech.Phys.Solids.* 15, 331-339.

[26] Swanson, S.R., 2004, Hertzian Contact of Orthotropic Materials, *Int. J. Solids Struct.* 41**,** 1945-1959.

[27] Vlassak, J.J., Ciavarella, M., Barber, J.R., Wang, X., 2003, The Indentation Modulus of Elastically Anisotropic Materials for Indenters of Arbitrary Shape, *J.Mech.Phys.Solids.*, 51, 1701-1721.

[28] Gradshteĭn, I.S., Ryzhik, I.M., edited by Jeffrey, A., Zwillinger, D., *Table of integrals, series and products* (2007).

APPENDIX A

In this appendix, several infinite integral values used are shown below,

$$\int_0^\infty \frac{\sin p}{p} J_1(p\tau)dp = \begin{cases} \dfrac{1}{\tau}, & 1 \le \tau \\[2mm] \dfrac{\tau}{1+\sqrt{1-\tau^2}}, & 1 \ge \tau \end{cases} \tag{A1}$$

$$\int_0^\infty \sin p J_0(p\tau)dp = \frac{1}{\sqrt{1-\tau^2}}, \quad \tau < 1 \tag{A2}$$

$$\int_0^\infty \frac{\cos p - 1}{p^2} J_1(p\tau)dp = \begin{cases} \dfrac{\tau}{2}[\log(\dfrac{\tau}{1+\sqrt{1-\tau^2}}) - \dfrac{1-\sqrt{1-\tau^2}}{\tau^2})], & \tau < 1 \\[3mm] -\dfrac{1}{2\tau} & \tau > 1 \end{cases} \tag{A3}$$

$$\int_0^\infty \frac{\cos p - 1}{p} J_0(p\tau)dp = \begin{cases} -\cosh^{-1}(\dfrac{1}{\tau}), & 0 \le \tau \le 1 \\[2mm] 0 & \tau \ge 1 \end{cases} \tag{A4}$$

$$\int_0^\infty \frac{\sin p}{p} J_0(p\tau)dp = \begin{cases} \sin^{-1}(\dfrac{1}{\tau}), & 1 \le \tau \\[2mm] \dfrac{\pi}{2}, & 1 \ge \tau \end{cases} \tag{A5}$$

$$\int_0^a r\cosh^{-1}(\frac{a}{r})dr = \frac{a^2}{2} \tag{A6}$$

$$\int_0^\infty \frac{1-\cos(p)}{p^2} J_0(p\tau)dp = \sin^{-1}(1/\tau) + \sqrt{\tau^2 - 1} - \tau, \quad \tau > 1 \tag{A7}$$

VITA

M.S. Chunliu Mao grew up in Anshan City, Liaoning Province, China. She finished her B.S. in the Department of Marine Engineering, Harbin Engineering University, Heilongjiang, China in July 2008. Then, she was enrolled in the Mechanical Engineering Department in Texas A&M University in 2008 in College Station, TX. Contact address:

Department of Mechanical Engineering

Texas A&M University

3123 TAMU

College Station TX 77843-3123.

E-mail: maocl2008@gmail.com

Tel: 979-422-0716